frontiers | Frontiers in Earth Science

TYPE Original Research
PUBLISHED 28 September 2022
DOI 10.3389/feart.2022.904914

OPEN ACCESS

EDITED BY
Silvina Guzman,
CONICET Instituto de Bio y Geociencias del NOA (IBIGEO), Argentina

REVIEWED BY
Karoly Nemeth,
Massey University, New Zealand
Dario Pedrazzi,
Spanish National Research Council (CSIC), Spain

*CORRESPONDENCE
Rigoberto Aguilar,
raguilar@ingemmet.gob.pe

SPECIALTY SECTION
This article was submitted to Volcanology, a section of the journal Frontiers in Earth Science

RECEIVED 26 March 2022
ACCEPTED 22 August 2022
PUBLISHED 28 September 2022

CITATION
Aguilar R, Arteaga D, Manrique N, van Wyk de Vries B, Cueva K, Taipe E, Guillou H and Scao V (2022), Quaternary volcanism in the Yura Monogenetic Field near Arequipa city, southern Peru. *Front. Earth Sci.* 10:904914. doi: 10.3389/feart.2022.904914

Quaternary volcanism in the Yura Monogenetic Field near Arequipa city, southern Peru

Rigoberto Aguilar[1]*, David Arteaga[1,2], Nélida Manrique[1], Benjamin van Wyk de Vries[3], Kevin Cueva[1], Edu Taipe[1], Hervé Guillou[4] and Vincent Scao[4]

[1]Instituto Geológico Minero y Metalúrgico, Observatorio Vulcanológico del INGEMMET, Arequipa, Perú, [2]Universidad Nacional de San Antonio Abad del Cusco, Facultad de Ingeniería Geológica, Minas y Metalúrgica, Cusco, Perú, [3]Université Clermont Auvergne, Laboratoire Magmas et Volcans UMR 6524 CNRS, OPGC IRD, Campus Universitaire des Cézeaux, Aubière, France, [4]Laboratoire des Sciences du Climat et de l'Environnement, CEA-CNRS-UVSQ, Université Paris-Saclay, Gif sur Yvette, France

Arequipa (Peru) is an area where volcanic activity has been persistent during the Quaternary. Studies carried out in this area have highlighted the emplacement of ignimbrite deposits, large volcanic clusters and stratovolcanoes. Monogenetic volcanism is also present, although poorly explored and studied. Due to its location over an ignimbrite plain and poor state of preservation, the only identified monogenetic cone in the Arequipa basin was the Nicholson volcano, while other monogenetic centers remained unknown. This lack of information about the recent volcanism can lead to inadequate definition of scenarios in a hazard assessment in the region. The present study has investigated monogenetic volcanism in the northwestern edge of the Arequipa basin based on geological survey, geochronology and geochemical data. Here, we report for the first time five small volcanic centers such as Yura Viejo, Ccapua, Uyupampa, El Chiral and Patacocha, which together with the Nicholson volcano form the Yura Monogenetic Field. Stratigraphic considerations and new $^{40}Ar/^{39}Ar$ ages allow us to place the eruptive activity in the Middle–Upper Pleistocene (*c.* 195–54 ka). Phreatomagmatic, Strombolian and effusive eruptions characterize the monogenetic activity of the field. As a result of these eruptions, small scoria cones, maars, and lava flows/coulées were generated. The eruptive products show ubiquitous olivine phenocryst-rich (<10 vol%) set in a fine pilotaxitic groundmass, suggesting rapid ascent of basaltic magmas to the surface controlled by the tectonic setting. The analyzed rocks lie in a narrow range of basaltic-andesite composition (50.9–55.6 wt% SiO_2) being the most mafic Pleistocene - Recent volcanic products identified in the Arequipa basin, along with the least differentiated magmas from the nearby Chachani volcanic cluster. This work shows how monogenetic volcanism can occur contemporaneous and closely spaced to larger volcanic clusters and active stratovolcanoes. We hope the information provided here will contribute to improve the risk management by highlighting the scenario of monogenetic eruptions that should be considered in the hazard assessment.

KEYWORDS
monogenetic field, central volcanic zone, Yura, Arequipa, Peru

1 Introduction

Monogenetic volcanic fields are important manifestations of volcanic activity that usually consist of a set of separate vents (volcanic emission centers) including several volcanic geoforms such as scoria cones, maars, tuff cones, tuff rings, lava domes, and lava flows (e.g., Connor and Conway, 2000; Connor et al., 2000; Németh, 2010; Németh and Kereszturi, 2015). The term 'monogenetic volcano' is used to designate a volcano that erupts during a single period of time (weeks, months or years) in which there is no evidence of a significant or long-lasting temporary interruption in eruptive activity (Macdonald, 1972; Williams and McBirney, 1979; Connor and Conway, 2000). It is important to note that even within a day the accumulating tephra may suffer some syn-eruptive erosion and remobilization of pyroclasts. This is especially valid in areas where rainfall or heavy wind action may coincide with the eruption. The generally small volume of magma emitted is produced by one short, sustained period of activity, then the volcano becomes extinct, and any further activity occurs through a different magma intrusion and new locations. Usually, in monogenetic volcanoes, the magma body rises rapidly (within hours to days) to the surface, so there is little interaction with crustal rocks; it is for this reason that most of these volcanoes emit basaltic magmas (Valentine and Gregg, 2008).

Small volumes and low-silica contents usually characterize monogenetic volcanism. Wörner et al. (2018) described four main constructional volcano types in the Central Volcanic Zone of the Andes (Figure 1C): 1) andesitic and dacitic composite stratovolcanoes, 2) large volcanic clusters that have erupted relatively wide compositional ranges from mafic andesites to dacites, 3) voluminous rhyodacitic ignimbrite fields, and 4) scarce, volumetrically insignificant, basaltic or basaltic andesitic, monogenic fields. In the southern Peruvian Andes, recent studies have focused on the understanding of Pleistocene-Holocene stratovolcanoes (e.g., Thouret et al., 2001; Harpel et al., 2011; Rivera et al., 2014: Samaniego et al., 2016), large volcanic clusters (Mariño et al., 2020; Aguilar et al., 2022) and ignimbrite fields (e.g., Paquereau-Lebti et al., 2006, 2008; Thouret et al., 2016). However, there are few studies on monogenetic volcanism (e.g., Siebe et al., 2006; Delacour et al., 2007; Galas, 2011). Regional scale geological maps published by INGEMMET (Geological Survey of Peru) indicate the presence of some single monogenetic centers of probable Quaternary age (e.g., Marhuas volcano, Chivay lava field) to the north of Arequipa (>90 km), but their eruptive histories remain unknown. In addition, it is likely that many other monogenetic centers have not yet been discovered.

Monogenetic volcanism in the Arequipa region has been important in terms of volume and extension, as is the case of the Andahua (composed of at least 22 cones), Huambo and Orcopampa monogenetic fields (e.g., Delacour et al., 2007, their Figure 1; Galas, 2011) compared to other monogenetic fields in southern Peru. In the Arequipa tectonic depression, only the Nicholson monogenetic volcano was previously known to exist (Delacour et al., 2007; Global Volcanism Program, 2013). Emplaced over the Arequipa Airport Ignimbrite (Paquereau-Lebti et al., 2006), this scoria cone is easily recognizable in aerial photographs or satellite images (Figures 1, 5). Tephra-fall deposits cropping out near the Uyupampa town were mapped as part of older deposits of the Chachani volcanic cluster (Aguilar et al., 2022) since there was not an identified source and because these tephra layers were covered by lava flows from one of the Chachani's edifices.

In this work, we present an overview of the Quaternary monogenetic volcanism near the Arequipa basin. We herein document for the first time the Yura Viejo, Ccapua, Uyupampa, El Chiral and Patacocha volcanoes, which together with the Nicholson cone may form what we name the "Yura Monogenetic Field". These small volcanoes composing the monogenetic field, the Chachani volcanic cluster and Misti stratocone border the Arequipa basin following a NW-SE trend (Figure 1B). Based on detailed fieldwork, satellite images and photogrammetry, whole-rock geochemistry and petrographic descriptions we characterize Nicholson, Ccapua, Yura Viejo, and Uyupampa volcanoes. Due to inaccessibility, we carried out a remotely-based analysis of El Chiral and Patacocha volcanic centers. Furthermore, combining field data and morphometric parameters we propose the eruption style and classification of each volcano in this monogenetic field, contributing to the understanding of monogenetic volcanism in southern Peru.

The Yura Monogenetic Field, located along the border of a tectonic basin, where the small monogenetic volcanoes were emplaced over ignimbrite deposits and near the Chachani large volcanic cluster and Misti stratovolcano, constitutes a very interesting example of monogenetic activity occurring in a temporal and spatial proximity to polygenetic volcanism with larger explosive and effusive eruptions. Reconstructing the history of volcanic activity around urban areas is fundamental for constraining the hazard scenarios and risk assessment.

2 Geological and tectonic setting

The magmatic and volcanic activity in the Peruvian segment of the Andean Central Volcanic Zone is ongoing since the Lower Jurassic (~190 Ma) until present (e.g., Mamani et al., 2010), but increased in Cenozoic times, especially during the uplift of the Andes after 40 Ma (e.g., Thouret et al., 2016). At the regional

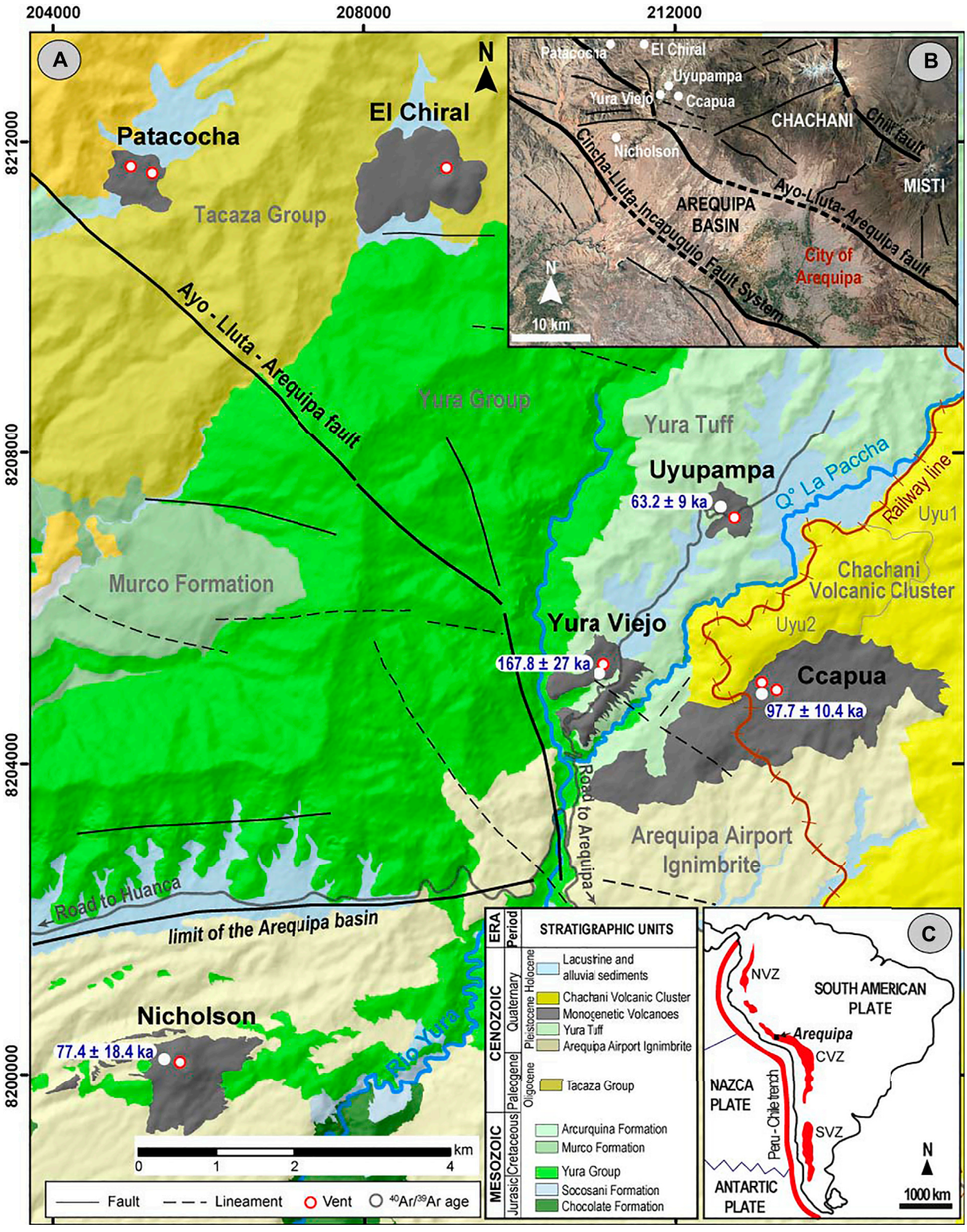

FIGURE 1
(A) Geological map of the Yura Monogenetic Field, northeastern of the Arequipa basin. Lithological data was taken from GEOCATMIN, INGEMMET (2014) and Paquereau-Lebti et al. (2006). Relief of image taken from Arc Map World Imagery Service. **(B)** Inset of a schematic map of the structural setting of the Arequipa basin and surrounding areas. **(C)** Inset of the subduction zone and convergence between Nazca and South American plates are indicated. Red polygons indicate the Northern (NVZ), Central (CVZ) and Southern (SVZ) Volcanic Zones respectively. Continuous and thick red line indicates the Peru-Chile Trench.

scale, Mamani et al. (2010) described the magmatism and geochemical evolution since 91 Ma, with overlap and migration of seven magmatic arcs during different periods. Tectonic shortening and magmatism allowed the thickening of the continental crust (Ramos, 2010; Armijo et al., 2015). The seven successive arcs are: 1) Toquepala (91–45 Ma), 2) Andahuaylas-Anta (45–30 Ma), 3) Tacaza (30–24 Ma), 4) Huaylillas (24–10 Ma), 5) Lower Barroso (10–3 Ma), 6) Upper Barroso (3–1 Ma) and 7) the Frontal Arc or Present-day Arc (<1 Ma). The active magmatic arc or "Frontal Arc" in southern Peru results from eruptive activity since ~1.3 Ma. The Pleistocene Frontal Arc (e.g., Mamani et al., 2010) is located 220–250 km east of the Peru-Chile Trench and above a 30°dipping slab (Thorpe et al., 1982; Wilson, 1986; Stern, 2004) (Figure 1). The present-day range of active, dormant and extinct volcanoes that grew upon the Western Cordillera along a N130° and N160°orientation parallels the Peru-Chile Trench (15° 15′-17° 30′S and 70° 00′-73° 30′W).

The geodynamic context includes an active continental margin and an archetypal Andean subduction (Thorpe et al., 1982; Wilson, 1986). However, in southern Peru, the continental magmatic arc is also obliquely convergent (i.e., the plate margin is at about N74 ± 4°E angle to the subduction direction; Norabuena et al., 1998). This oblique convergence is accommodated since at least the Neogene by sinistral faults (Mering et al., 1996; Sempere et al., 2014). Neogene to Recent volcanism is often associated with trans-tensional regimes because these areas offer less resistance through normal and strike-slip faults, through which the magma can rise more easily to the surface (e.g., van Wyk de Vries and Merle 1998; Acocella et al., 1999).

The WNW-ESE oriented Arequipa depression (Figure 1B) has been interpreted as a pull-apart basin associated with regional ~N130° transtensive faults (Mering et al., 1996; Thouret et al., 2001; Benavente et al., 2017). The basin is filled by Middle Miocene to Early Pleistocene ignimbrites (e.g., Paquereau-Lebti et al., 2006), and more recent volcanoclastic deposits and alluvial deposits. The basin boundary is formed by the Cincha-Lluta-Incapuquio Fault System (Figure 1B) which has experienced different tectonic regimes (Vicente et al., 1982), delineating the western limit of the Western Cordillera, and has influenced the sedimentation of the Arequipa basin (e.g., Carlotto et al., 2009). Studies conducted around the Arequipa basin have shown that this fault system has operated during the Mesozoic in successive extensional and reverse regimes (e.g., Acosta et al., 2010). The system was interpreted as transpresive faults (Vicente et al., 1982), which now act in a trans-tensional regime.

The N130° oriented Ayo-Lluta-Arequipa Fault (also known as Huanca fault) is a regional structure that was formerly a thrust fault. This structure brings into contact Mesozoic sedimentary units (including the Yura Group) with the Cenozoic volcano-sedimentary units (Figure 1). During the Cenozoic, the area was affected by major compressive phases. Since the Middle Miocene, extensional tectonics has had a major influence on volcanism in the Western Cordillera (Huaman Rodrigo et al., 1985 in Mering et al., 1996). Since the Pliocene, the Ayo-Lluta-Arequipa system has acted as a normal and sinistral fault (Mering et al., 1996; Sempere and Jacay, 2006).

2.1 The bedrock stratigraphy of Yura Monogenetic Field

Several of the pyroclastic deposits in the Yura Monogenetic Field contain rock fragments extracted from the substrate on which the volcanoes were emplaced. In the area surrounding the Yura town, the bedrock is formed of Mesozoic sedimentary and Neogene volcanic deposits (Figure 1). A summary of stratigraphic units of the bedrock is presented in Table 1.

3 Methods

3.1 Geological mapping and sample collection

Fieldwork was carried out during short field campaigns between June 2018 and November 2021. We visited 114 field sites distributed in the monogenetic field along the Yura Valley (Figure 1). The source of individual lava flows and pyroclastic deposits was distinguished by using stratigraphic and volcanological relationships between deposits and geoforms (scoria cones, maars, fissures that fed flows or topographic highs). Mapping of eruptive units (1:25000 scale) included lithologic criteria (type, size, and abundance of mineral phases) and morphologic criteria (e.g., Condit and Connor, 1996). Outcrops in natural surfaces together with road-cuts and quarries served to carry out the facies observations and descriptions. Four stratigraphic logs were measured in outcrops with greater exposure of stratigraphic units. The geological maps of the Yura Monogenetic Field were digitized using ArcMap® 10.1 (https://desktop.arcgis.com) at 1:25000 scale, the same scale used by INGEMMET (Instituto Geológico Minero y Metalúrgico) for geological maps of active volcanoes in Peru. The coordinate system of all maps presented herein are UTM WGS84, Zone 19S. Polygons delimiting the volcanoes were used to calculate their surface areas in ArcMap. In some areas, high-resolution digital elevation models (UTM-WGS84 DEM, 60-cm spatial resolution) were obtained by oblique photogrammetry with a Phantom-4PRO drone. The methodology of photogrammetry was similar to that described by Diefenbach et al. (2012) and James et al. (2020). We used AgiSoft Photoscan® software (https://www.agisoft.com) for photogrammetric analysis. Morphometric parameters described by Wood (1979) such as cone basal diameter, crater diameter and cone height were obtained from fieldwork data and high-resolution DEMs

TABLE 1 Bedrock in the surrounding areas of the Yura Monogenetic Field.

Unit	Description	Age	Reference
Chachani Volcano Cluster	Consist of at least twelve volcanic edifices forming a group of stratovolcanoes, dome coulées and blocky-lava flow fields. Their deposits overly the Arequipa Airport Ignimbrite and the Yura Tuff, and a lava flow in its western flank partially covers the Ccapua monogenetic volcano.	1012 ± 53–56.5 ± 31.6 ka	Aguilar et al. (2022)
Yura Tuff	Non-welded pumice and ash pyroclastic flows the volume of which was estimated at ~1.5 km^3. Yura Tuff outcrops are restricted to the north and west sides of Chachani complex. They fill a north-south elongated depression between sediments of the Yura Group and Pre-Chachani lava bedrock	1.278 ± 46 Ma	Paquereau-Lebti et al. (2006, 2008). Aguilar et al. (2022)
Arequipa Airport Ignimbrite	Consists of two units (18 km^3), a white indurated massive ash-and-lapilli tuff overlain by a pink non-welded, massive and lithic-rich lapilli tuff. The source of this ignimbrite is buried under the Chachani Volcano Cluster, as indicated by Anisotropy of Magnetic Susceptibility measurements and the size of lithic fragments, which increases towards the north	1.65 ± 0.04 Ma	Paquereau-Lebti et al. (2006, 2008)
Tacaza Group	Composed of volcanic breccia and andesitic lavas. These volcanic rocks crop out in the northwestern part of the study area	Oligocene	Jenks (1946)
Arcurquina Fm	Composed of marine, regularly-bedded, thickening-upward, grey to black, organic rich micritic limestones. These rocks are found to the northwestern side of the study area	Middle to Upper Cretaceous (Albian to Cenomanian)	Jenks (1948); Callot et al. (2008)
Murco Fm	Mainly composed of dark shales and soft chert with a predominance of variegated sandstones. These sequences are found forming the flanks of the anticlines and synclines of the area. The outcrops of this formation are found in the western part of the monogenetic field	Middle Cretaceous	Wilson (1963)
Yura Group	Sedimentary rocks from floodplain deposits and lateral accretion of point-bar deposits sited on a semi-flat topography. The outcrops are found in the central part, near the monogenetic volcanoes	Middle to Late Jurassic (Callovian to Tithonian)	Benavides (1962); Alván et al. (2018)
Socosani Fm	Consist of shales interbedded with fossiliferous limestones. These rocks crop out along the Río Yura, to the southeast of Nicholson volcano.	Middle—Upper Jurassic	Benavides (1962)
Chocolate Fm	Composed of purplish volcanic and sedimentary (sandstone and limestone) rocks, some of which have been affected by metamorphism. The outcrops of Chocolate Fm. are found in the southern part of the area	Lower Jurassic	Vargas (1970)

using ArcMap. The average flank slopes were calculated trigonometrically using the morphometric parameters (e.g., Hasenaka and Carmichael, 1985).

3.2 Petrography, geochemistry and geochronology

Twelve lava and scoria samples were used for petrographic descriptions. Thin sections of those samples were studied in order to describe representative rocks from the volcanic centers. Ten of them have been taken in volcanic deposits (bombs and lavas), while two are xenoliths included in tephra-fall deposits. Given that the mineral assemblage is quite homogeneous, the number of samples is deemed representative. All analyzed samples are fresh, or at least show no conspicuous weathering. Modal analyses of the sample set are given in Table 2. The abundance of each main mineral phase in thin section was determined by using images taken with a polarized microscope in the most representative zones. Using Adobe® Illustrator (https://www.adobe.com/la/products/illustrator.html), the images were examined to determine the percentage of each mineral. For determining the frequency (modal analysis), we used the point-counting method (e.g., Rodríguez Rey et al., 2004) following five steps: 1) we consider a rectangular frame inside the image to restrict the crystal counting to this area. Two sides of the frame have dashed lines and the other have continue lines. 2) All crystals that were completely included within the frame and the crystals that have some portion inside the dashed lines were counted (point counting). 3) Into the rectangular frame, we added a grid of 600 points. 4) Each point intersecting a crystal was manually counted to calculate the number of crystals contained in the frame. 5) The % abundance is obtained by: (# of crystals/Area of rectangular frame) × 100.

Major and trace element analyses of whole-rock samples were performed by ICP-AES and ICP-MS respectively, with an analytical precision (2σ) less than 1% for major elements and around 5% for trace elements at Instituto Geológico Minero y Metalúrgico (INGEMMET) in Peru. For these analyses, agate-crushed powders of seventeen samples were mixed with $LiBO_2$, placed in a graphite crucible, and melted in an induction oven at 1050°C for 4.5 min, resulting in a homogeneous glass bead. The glass was then

TABLE 2 Summary of the petrographic characteristics of the Yura monogenetic field. Pl: plagioclase, Px: pyroxene, Amph: amphibole, Qz: quartz, Op: opaques, Cb: carbonates, Kfd: potasic feldspar. % values in parentheses represents the percentage of crystal content as phenocrysts (>500 μm) and micro-phenocrysts (100–500 μm) and microlites (<100 μm) in the groundmass.

Volcano	Sample	Mineral assemblage				Texture		Deposit type	Rock type (modal classification)	Observations
		Crystals		Groundmass (% vol.)	Alteration mineral (% vol.)	Whole rock	Mineral			
		Phenocryst (% vol.)	Accessory (% vol.)							
Nicholson	CHA-VR21-010	Ol (~9)	Op (~4)	Px (~42) ± Pl (~38) ± glass (~2) ± vesicles (~5)	-	Porphyritic, pilotaxitic groundmass	Ol skeletal growth, glomeroporphyritic	Scoria fall	Basaltic andesite	Irregular vesicles, xenoliths (volcanic)
Ccapua	CHA-VR21-001	Ol (~7)	Op (~4)	Pl (~32) ± Px (~25) ± glass (~4) ± vesicles (~27)	clay (~1)	Porphyritic, pilotaxitic groundmass	Ol skeletal growth, glomeroporphyritic	Scoria fall	Basaltic andesite	Irregular vesicles
	CHA-18-25	Ol (~8)	Op (~3)	Pl (~30) ± Px (~22) ± Ol (~5) ± glass (~5) ± vesicles (~27)	-	Porphyritic, pilotaxitic groundmass	Ol skeletal growth, glomeroporphyritic	Lava flow	Basaltic andesite	Sub-rounded vesicles
	CHA-18-50	Ol (~10)	Op (~4)	Pl (~31) ± Px (~23) ± glass (~4) ± vesicles (~28)	Fe ox (traces)	Porphyritic, pilotaxitic groundmass	Ol skeletal growth, glomeroporphyritic	Scoria fall	Basaltic andesite	Irregular vesicles
	CHA-19-51	Ol (~9)	Op (~4)	Pl (~34) ± Px (~26) ± glass (~2) ± vesicles (~25)	Fe ox (traces)	Porphyritic, pilotaxitic groundmass	Ol skeletal growth, glomeroporphyritic	Scoria fall	Basaltic andesite	Irregular vesicles
Yura Viejo	CHA-VR21-002	Ol (~6)	Op (~4)	Px (~34) ± Pl (~25) ± glass (~3) ± vesicles (~28)	clay (traces) ± Fe ox (traces)	Porphyritic, pilotaxitic groundmass	Ol skeletal growth, glomeroporphyritic	Scoria fall	Basaltic andesite	Irregular vesicles
	CHA-18-46	Ol (~9)	Op (~4)	Px (~28) ± Pl (~26) ± glass (~4) ± vesicles (~29)	clay (traces)	Porphyritic, pilotaxitic groundmass	Ol skeletal growth, glomeroporphyritic	Scoria fall	Basaltic andesite	Irregular vesicles, volcanic enclaves
	CHA-VR21-004	Ol (~9)	Op (~3) ± Amph (traces)	Px (~34) ± Pl (~31) ± glass (~2) ± vesicles (~21)	opacite (traces) ± clay (traces)	Porphyritic, trachytic groundmass	Ol skeletal growth, glomeroporphyritic	Scoria fall	Basaltic andesite	Irregular vesicles
	CHA-VR21-003A	Qz (~87)	Op (~2) ± Kfd (~1) ± zr (traces)	clay (~4) ± Cb (~2)	-	Clastic	-	sedimentary xenolith	quartz sandstone	Volcanic lithic fragments, Siliceous lithic fragments
	CHA-VR21-003B	Qz (~85)	Kfd (~1) ± Op (traces) ± zr (traces)	clay (~11)	-	Clastic	-	sedimentary xenolith	quartz sandstone	Volcanic lithic fragments
Uyupampa	CHA-VR21-009	Ol (~8)	Op (~6)	Pl (~53) ± Px (~20) ± glass (traces) ± vesicles (~13)	-	Porphyritic, trachytic groundmass	Ol skeletal growth, coronitic	Lava flow	Basaltic andesite	Irregular vesicles
	CHA-18-26	Ol (~9)	Op (~3)	Pl (~32) ± Px (~28) ± glass (~2) ± vesicles (~26)	clay (traces) ± opacite (traces)	Porphyritic, pilotaxitic groundmass	Ol skeletal growth, coronitic	Scoria fall	Basaltic andesite	Irregular vesicles, sedimentary xenolith

dissolved in a solution of deionized water and nitric acid (HNO_3) and finally diluted by a factor of 2000. For comparison with surrounding volcanic products, these new data (Table 3) were combined with previously analysed rock samples from Chachani volcano cluster (Mamani et al., 2010; Aguilar et al., 2022), Arequipa Airport Ignimbrite and Yura Tuff (Paquereau-Lebti et al., 2006).

The chronology of volcanic activity in the Yura Monogenetic Field was constrained using the $^{40}Ar/^{39}Ar$ dating method at the Laboratoire des Sciences du Climat et de l'Environnement (LSCE/IPSL, Gif-sur-Yvette, France). Groundmass in the samples from Yura Viejo, Uyupampa, Ccapua and Nicholson volcanoes were used for age determinations. $^{40}Ar/^{39}Ar$ ages are summarized in Table 4, whereas, the corresponding analytical procedures and results are detailed in the Supplementary Material S1, S2.

4 Volcanism and crustal structure in the yura monogenetic field

4.1 Volcanic activity

The Yura Monogenetic Field is composed of six volcanic centers; three of them (Patacocha, Yura Viejo and Ccapua) are

TABLE 3 Major, trace and REE analyses of samples from Arequipa Airport Ignimbrite (AAI), Yura Tuff and Yura Monogenetic Field obtained during this work. All Fe is given as Fe_2O_3. The coordinates of the sample locations are indicated in UTM WGS84, Zone 19S.

Unit	AAI	Yura tuff								Ccapua				Nicholson	Uyupampa		Yura Viejo								
Sample	CHA-18-19	CHA-18-58B	CHA-18-27	CHA-18-52	CHA-18-53	CHA-19-48	CHA-19-45	CHA-19-47	CHA-VR21-005	CHA-18-25	CHA-19-50	CHA-19-51	CHA-VR21-001	CHA-19-52	CHA-18-26	CHA-R21-009	CHA-VR21-002	CHA-VR21-004	CHA-VR21-012a	CHA-VR21-012b	CHA-VR21-012c	CHA-VR21-012d	CHA-VR21-012e	CHA-VR21-012f	CHA-R21-012g	CHA-R21-012h
Type	pumice 214187	pumice 218335	pumice 214839	pumice 9214864	pumice 9214864	pumice 214275	pumice 212382	pumice 214770	pumice 218032	scoria 211989	scoria 213177	lava flow 213207	scoria 213209	lava flow 205935	scoria 212710	lava flow 212688	scoria 210536	lava flow 211218	scoria 211280	scoria 211280	scoria 211280	scoria 211280	scoria 211280	scoria 211280	scoria 211280	scoria 211280
East																									
North	8201556	8216174	8212280	8210161	8210161	8213944	8204788	8220951	8213226	8204176	8204984	8205007	8205215	8200162	8207154	8207175	8204358	8205159	8205224	8205224	8205224	8205224	8205224	8205224	8205224	8205224
SiO_2	72.5	69.9	71.4	71.7	71.5	72.1	68.3	67.9	67.1	50.9	53.5	54.4	55.6	51.3	53.3	55.0	55.6	53.2	54.5	54.2	54.0	54.5	54.2	54.5	54.4	54.9
TiO_2	0.15	0.20	0.18	0.19	0.20	0.12	0.29	0.27	0.56	1.56	1.43	1.40	1.36	1.48	1.37	1.46	1.40	1.39	1.32	1.35	1.36	1.37	1.35	1.37	1.37	1.36
Al_2O_3	12.7	13.3	13.3	12.6	12.5	13.7	14.2	14.4	13.1	16.4	16.8	16.8	15.6	15.7	16.5	15.6	14.8	15.6	16.8	16.9	16.8	16.8	16.7	16.6	16.6	16.8
Fe_2O_3	1.03	1.15	1.12	1.23	1.21	0.91	1.95	1.85	3.44	10.26	8.28	8.40	8.26	9.88	8.79	8.58	8.93	8.86	8.55	8.55	8.76	8.62	8.73	8.69	8.64	8.68
MnO	0.08	0.05	0.08	0.07	0.07	0.07	0.06	0.06	0.06	0.14	0.10	0.10	0.11	0.13	0.13	0.12	0.12	0.12	0.15	0.14	0.15	0.14	0.16	0.16	0.15	0.15
MgO	0.24	0.35	0.31	0.38	0.41	0.16	0.70	0.61	1.74	5.31	4.48	4.49	4.07	5.95	4.94	4.40	4.62	4.49	4.27	4.12	4.31	4.14	4.18	4.29	4.33	4.14
CaO	0.88	1.15	1.06	1.45	1.31	1.01	2.05	1.39	2.86	8.19	7.61	7.57	7.02	8.08	7.56	7.11	7.25	7.16	7.50	7.50	7.53	7.50	7.54	7.59	7.64	7.51
Na_2O	3.73	3.04	3.53	3.47	3.70	3.92	4.17	3.66	2.91	3.87	4.35	4.21	3.96	3.47	3.96	4.00	3.58	3.95	4.03	4.02	4.03	4.06	4.08	4.14	4.09	3.99
K_2O	4.03	4.80	4.45	4.08	4.02	4.05	3.87	4.20	4.01	1.77	2.01	1.99	1.81	1.60	1.79	1.84	1.58	1.81	1.88	1.90	1.84	1.87	1.88	1.87	1.91	1.89
P_2O_5	0.07	0.06	0.10	0.08	0.08	<0.01	0.11	0.09	0.18	0.40	0.45	0.40	0.42	0.33	0.42	0.43	0.34	0.41	0.41	0.42	0.45	0.42	0.42	0.44	0.45	0.44
LOI	3.48	6.01	4.08	3.74	4.07	3.12	4.18	4.54	2.59	0.78	0.33	0.15	<0.01	0.71	0.46	0.10	0.17	0.95	0.42	0.50	0.43	0.38	0.23	0.37	0.47	0.12
Rb		141		54	76	110	85	104	115		35	35	50	25	44	31	41	43	47	41	41	45	45	46	45	45
Sr	111	205	186	155	170	167	311	202	428	881	953	982	913	886	892	900	844	943	870	755	824	823	824	852	778	824
Y	15	10	16	16	16	14	15	15	22	20	17	16	17	18	18	37	18	31	20	19	18	17	17	17	16	16
Nb	10.3	9.1	10.4	11.1	11.2	11.7	8.6	10.6	8.5	5.1	6	5.8	7	5.2	5.7	7.6	6.4	6.7	6.7	6.4	6	6.1	6	5.8	6.1	6.6
Zr	110	165	121	144	140	110	127	174	172	155	91	110	145	89	161	176	164	173	188	160	124	150	139	129	146	178
Cs	1.56	3.82	1.81	1.67	1.68	2.49	1.45	1.69	2.27	0.42	0.51	0.44	0.4	0.83	0.49	0.37	0.49	0.37	0.59	0.83	0.63	0.57	0.68	0.59	0.73	0.61
Ba	1092	1094	1186	757	959	930	1079	889	1064	740	898	913	767	630	836	786	630	786	907	798	868	848	873	883	809	839
Hf	3.6	4.6	3.7	4	4	3.7	3.9	5.2	5.4	3.8	3.9	3.8	4	3.4	4	4.9	4.6	4.7	4.8	4.1	3.2	4	3.5	3.2	3.6	4.1
Th	10.1	17.8	10	10.4	10.5	9.9	7.7	9.7	9.1	1.8	2.6	2.4	3.3	2	2.2	3.3	3.1	2.9	2.9	2.8	2.7	2.7	2.8	2.6	2.6	3.2
U	1.4	3.1	1.4	1.4	1.3	1.5	1.2	1.2	1.4	0.4	0.5	0.5	0.5	0.4	0.4	0.5	0.5	0.4	0.6	0.6	0.6	0.6	0.6	0.5	0.6	0.6
La		43		15	27	24	33	27	37		36	36	33	28	33	32	29	34	39	33	36	36	37	38	34	36
Ce	86.3	90.6	78.8	84	82.4	83	75.7	84.9	78.5	68.5	80.5	79.5	81.1	59.4	76.6	78.4	71.6	80.9	82.4	81.5	81.2	78.8	81.3	79.3	83	81.5
Pr	8.5	8.6	7.5	8.3	8.1	8.8	8.1	8.9	9	7.6	10	9.7	10.1	7.7	8.2	10.2	9	10.2	10.1	10	9.8	9.8	9.9	9.6	10.1	9.8
Nd	31.4	28.3	28.2	27.5	27.1	30.1	28.2	30.7	31.8	36.4	40	40.1	40.6	32.4	38.1	40.7	37.8	40.8	41.3	40.1	40.5	39.9	40.5	39.4	40.3	39.8
Sm	4.4	4	4.2	4.3	4.1	5	4.2	4.8	5.1	6.4	7.2	7.2	7.3	6.6	6.7	7.3	7.2	7.2	6.9	6.9	6.7	6.8	6.7	6.8	6.8	7
Eu	0.8	0.8	0.8	0.8	0.8	0.9	1	0.9	1	1.8	1.9	1.8	1.8	1.7	1.7	1.8	1.7	1.8	2	1.9	1.8	1.8	1.8	1.9	1.9	1.8
Gd	3.3	2.8	3.2	3.4	3.1	3.4	3.2	3.5	3.9	5.9	6	5.7	5.9	5.6	5.4	5.9	6.4	5.7	6	6	5.8	5.7	5.7	5.7	5.7	5.9
Tb	0.4	0.3	0.4	0.4	0.5	0.5	0.4	0.5	0.5	0.8	0.8	0.7	0.8	0.8	0.7	0.8	0.9	0.8	0.8	0.8	0.8	0.7	0.7	0.7	0.7	0.7
Dy	2.5	1.8	2.7	2.6	2.5	2.8	2.6	2.9	2.4	4.4	4.2	4.1	3.7	4.3	3.9	3.7	4.2	3.7	3.8	3.8	3.5	3.6	3.7	3.5	3.6	3.6
Ho	0.4	0.3	0.4	0.5	0.5	0.5	0.5	0.5	0.5	0.7	0.7	0.7	0.7	0.8	0.6	0.7	0.8	0.7	0.7	0.7	0.7	0.7	0.7	0.7	0.7	0.7
Er	1.4	0.9	1.5	1.4	1.4	1.5	1.4	1.6	1.4	2	2	1.9	1.8	2.2	1.7	1.8	2.2	1.8	1.8	1.7	1.7	1.6	1.6	1.6	1.6	1.6
Tm	0.2	0.1	0.2	0.2	0.2	0.2	0.2	0.2	0.2	0.3	0.2	0.2	0.2	0.3	0.2	0.3	0.3	0.2	0.2	0.2	0.2	0.2	0.2	0.2	0.2	0.2
Yb	1.5	0.8	1.7	1.6	1.5	1.5	1.4	1.5	1.4	1.8	1.5	1.5	1.5	1.8	1.5	1.6	1.7	1.5	1.4	1.4	1.5	1.5	1.5	1.4	1.4	1.5
Lu	0.2	<0.15	0.21	0.21	0.2	0.22	0.21	0.23	0.21	0.22	0.23	0.22	0.21	0.26	0.2	0.21	0.25	0.21	0.21	0.2	0.2	0.22	0.2	0.2	0.21	0.21

10.3389/feart.2022.904914

TABLE 4 Summary of $^{40}Ar/^{39}Ar$ data from incremental heating experiments on groundmass splits.

Sample Lab file #	Volcano	Type of deposit	UTM Easting	UTM Northing	wt. (mg)	K/Ca (total)	Total FusionAge (ka)	Age Spectrum				Isochron analysis				
								Increments used (°C)	^{39}Ar (%)	Age ± $2\sigma^{(1)}$ (ka)	$^{40}Ar/^{36}Ar$ ± $2\sigma^{(1)}$ MSWD	n/ N	MSWD	$^{40}Ar/^{36}Ar$ ± $2\sigma^{(1)}$ intercept	Age ± $2\sigma^{(1)}$ (ka)	F Spreading Factor
CHA-VR21-09																
FG-2995 to FG-3003	Uyupampa	lava flow	213209	8205215	131	0.36	51.6 ± 10.6	726–1081	88.3	**63.2 ± 9.0**	0.37	7 of 9	0.67	298.3 ± 2.4	65.3 ± 17.5	3.4%
CHA-VR21-010																
FG-3004 to FG-3013	Nicholson	scoria fall	205497	8200259	131	0.28	79.7 ± 20.8	663–1083	98.0	**77.4 ± 18.4**	0.24	8 of 10	0.43	299.5 ± 2.0	63.4 ± 31.8	1.4%
CHA-VR21-001																
FG-2984 to FG-2993	Ccapua	scoria fall	213209	8205215	124	0.41	99.5 ± 13.8	725–1167	98.7	**97.7 ± 10.4**	0.16	8 of 10	0.20	299.0 ± 3.3	95.8 ± 19.6	6.7%
CHA-VR21-004																
FG-3014 to FG-3023	Yura Viejo	lava flow	211218	8205159	121	0.23	133.9 ± 28.0	788–1168	84.4	**167.8 ± 27.0**	0.32	7 of 9	0.52	298.8 ± 3.3	164.6 ± 59.8	2.9%

Ages calculated relative Acs-2 at 1.1891 Ma (Niespolo et al., 2017) and the total ^{40}K decay constant of Renne et al. (2011). (1): Full external error. n/M: number of crystals retained in the age calculation over the number of analyzed crystals. F: Spreading factor of Jourdan et al. (2009). Values in bold indicate the ages considered for each volcano.

10.3389/feart.2022.904914

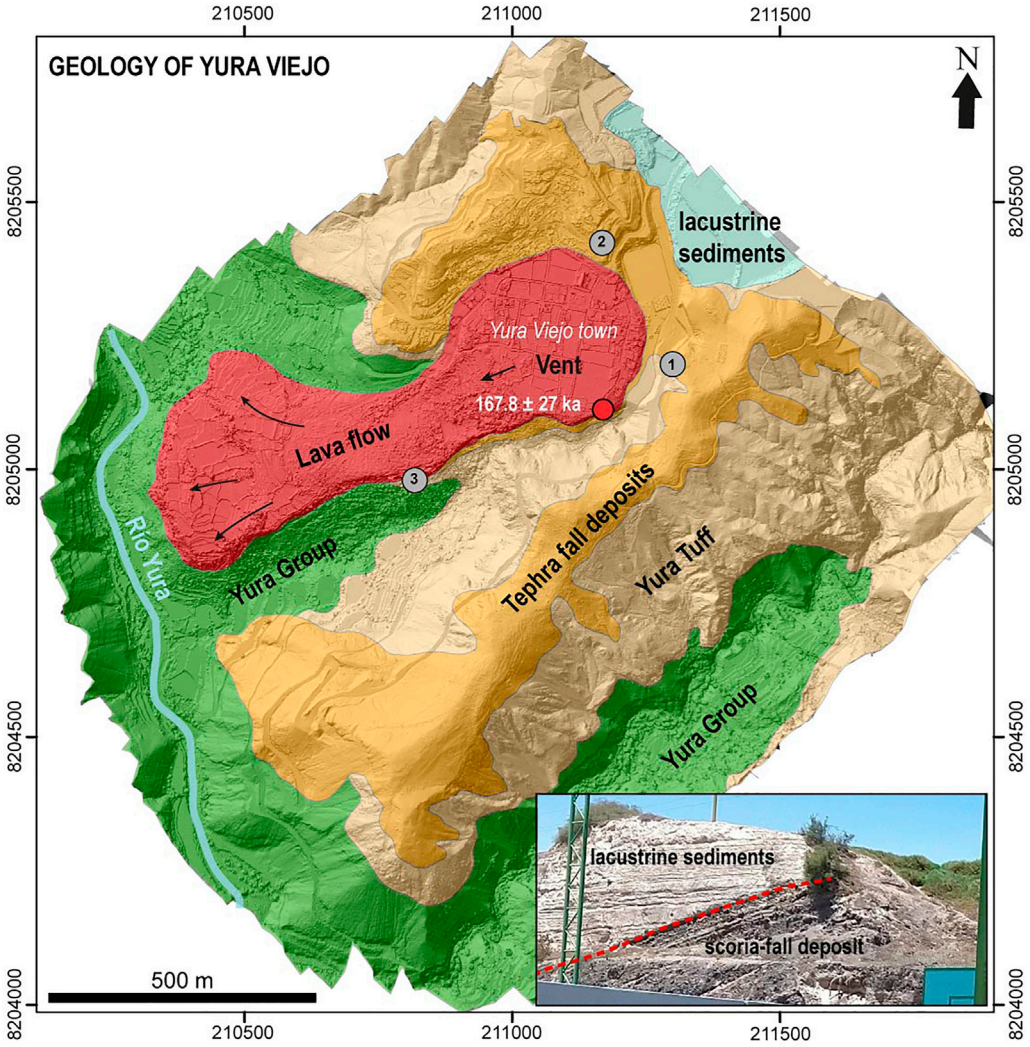

FIGURE 2
Geological map of the Yura Viejo volcano, embedded on a 60-cm resolution digital Elevation Model (DEM) map. Gray numbered dots indicate the location of stratigraphic sections shown in Figure 5. In the lower-right corner, a photograph of tephra fallout beds covered by lacustrine sediments.

distributed along ~10 km in a N130° direction, and two volcanic centers (El Chiral and Uyupampa) follow a N140° trend separated by 6 km, aligned with the Ayo-Lluta-Arequipa Fault. The Nicholson volcano is located near the northwestern limit of the Arequipa basin. Eruptive activity has been characterized by eruptions that generated scoria flows, pyroclastic fallout and lava flow emissions.

4.1.1 Yura Viejo

This volcano was built above Yura Tuff and Mesozoic sedimentary rocks of the Yura Group (Figure 2). The crater (~520 m diameter) is situated in the current location of the town of Yura Viejo, which is marked by a semi-circular structure opened to the southwest. The preserved deposits cover an area ~0.74 km^2 surrounding the emission center. Three stratigraphic columns in the crater ring allowed us to describe its eruptive history, which is characterized by a succession of pyroclastic (PDC) scoria flows, scoria fallouts and reworked ash layers, ending with a lava flow deposit (Figures 2, 3). The pyroclastic components are mainly the same in all of the deposits, distributed in different sizes and proportions.

In the eastern flank (Figure 3, profiles 1 and 2), the lower successions, up to 12.50 m thick (thickness from the surveyed profiles), directly overlie the Yura Tuff along an erosional surface, and form the basal part of the ejecta ring on the eastern flank. These successions are characterized by scoria flows (10–150 cm thick), interbedded with bombs and lapilli fallout (20–80 cm thick), and ash layers (2–18 cm thick).

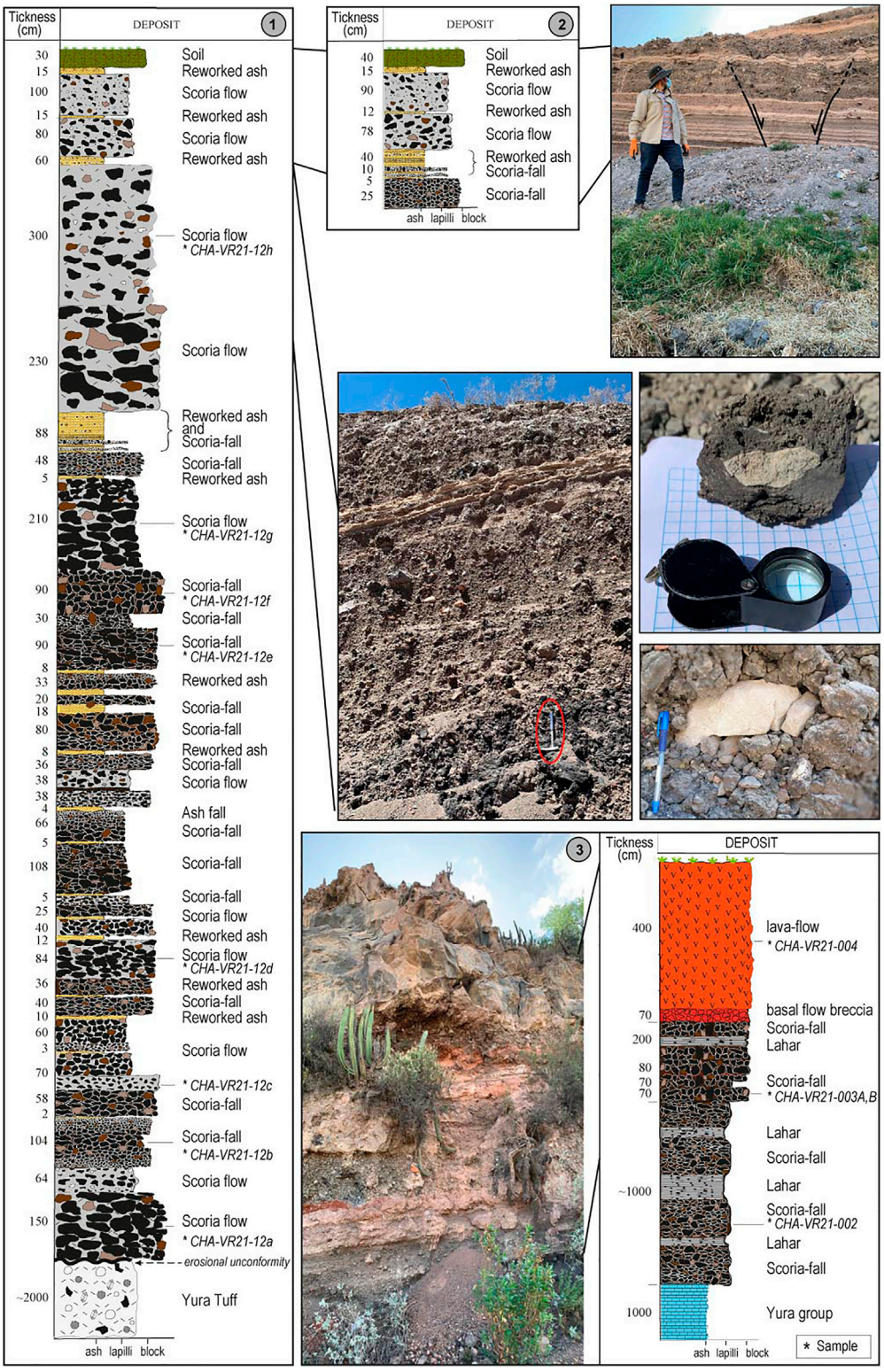

FIGURE 3
Stratigraphic sections described in outcrops of the Yura Viejo volcano. Photographs of outcrops of stratigraphic columns and the xenoliths included in the scoria blocks and fallout deposit. Black clasts in the deposits indicate the scoria, whereas the other colors indicate the lithics (sedimentary and rare ignimbrite lithics). The numbers (1, 2 and 3) indicate the location of the sections in Figure 2.

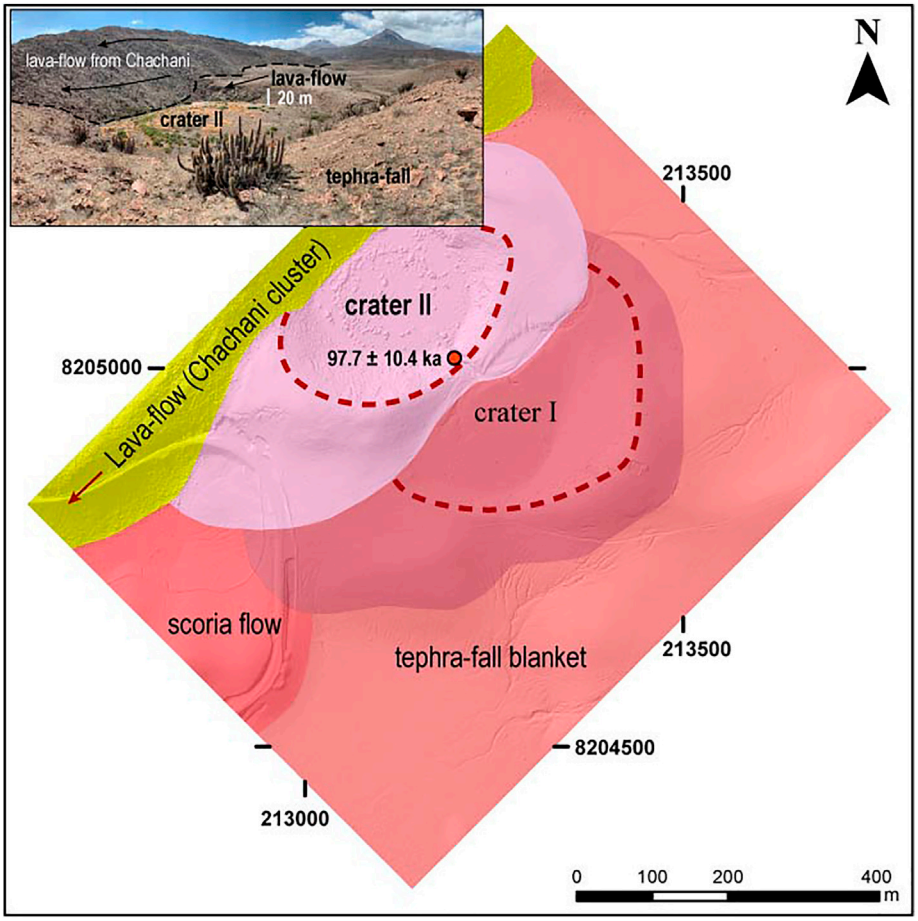

FIGURE 4
Geological map of Ccapua maar, embedded on a 60-cm resolution digital Elevation Model (DEM) map. On the upper-left corner, a photograph of crater II partially covered by a blocky lava flow from Chachani volcano cluster (Aguilar et al., 2022).

The scoria-flow deposits are composed of moderately to weakly indurated, unsorted, dark gray in color, and mostly clast-supported deposits. Sub-angular blocks (40–80%) are embedded in a medium-to-coarse ash matrix (20–60%). Juvenile clasts consist of scoria blocks (20–75%, 12–70 cm maximum size), dense lava blocks (<3%, <8 cm diameter), and bread-crust bombs (<2%, <200 cm diameter). Lithics are composed of quartz-sandstone, shale, and rare ignimbrite fragments (3–8%, 3–40 cm maximum size), which are found both included in scoria blocks (xenoliths) and loose fragments (Figure 3).

Block and lapilli fallout beds are moderately to well sorted, clast-supported, non-agglutinated, and have variable thicknesses (20–80 cm). The juvenile scoria of these layers are dark gray; the size of scoria fragments varies from 2 to 50 cm, and rare dense lava fragments (1–10 cm) are also found. The lithics are composed of quartz sandstone and shale from Yura Group, with variable maximum size (10–40 cm) and scarce ignimbrite fragments depending on the layer's thickness. These rocks are also incorporated as xenoliths in juvenile blocks. The ash layers are pinkish-gray in color, and have variable thickness in the log, from 2 to 18 cm in the lower layers, and up to 18 cm in the upper layers.

The upper succession is 11.60 m thick (from surveyed profiles), and consists predominantly of scoria flows, interbedded with ash-fall (mainly remobilized) and few block-and-lapilli fallout layers. The scoria flows are massive, unsorted, matrix-supported and dark gray deposits composed of blocks (30–40%) embedded in a fine matrix (60–70%). Blocks are scoria (22–30%, 15–60 cm maximum size), and quartz-sandstone and shale lithics (3–10%, 20–75 cm maximum size). Two block-fallout deposits are 48 cm and 90 cm thick respectively. Scoria blocks have maximum sizes of 7 and 50 cm, while sedimentary lithics are 20 cm in diameter. Ash fall layers are pinkish gray in color, moderately welded, and their thickness vary from 5 to 62 cm. Bread-crust scoria bombs reaching diameters up to 50 cm are found at ~1 km from the vent.

Described (successions) pyroclastic deposits in the eastern flank are not well-preserved in the southwestern flank (Figure 3, profile 3). However, scoria block fallouts interbedded with lahar flow deposits crop out over dark shale and sandstones strata from the Yura Group (Figures 2, 3) in a topographic low in this zone. Scoria-fall deposits are similar to those described above, whereas lahar flow deposits (1–2 m thick) are matrix-supported, compacted, pink and contain scoria fragments embedded in a muddy fine matrix. Superimposed on these deposits, a massive, dark-gray, a'a lava flow (~15 m thick) dated by $^{40}Ar/^{39}Ar$ at 167.8 ± 27.0 ka (Table 4) was emplaced filling a small valley oriented to the southwest, reaching a distance of ~1 km from the crater (Figure 2). This lava flow shows a brown basal breccia of <70 cm thick. This volcano was probably emplaced in an ancient riverbed, forming a dam where lacustrine sediments were accumulated. These sediments overlap the scoria-fall deposits in the northeastern side of the volcano (Figure 2).

Due to its resistance to erosion, the lava emitted by the Yura Viejo volcano is well preserved, and the ravine that previously existed in the area opened up on its sides, forming an elevated plateau (relief inversion process). On the other hand, the tephra generated by the explosions are readily eroded, and are currently found only in the upper part of the surrounding hills. Deposits of Yura Viejo are cut by NW-SE active faults, in areas close to the vent (Figure 3).

4.1.2 Ccapua

This eruptive center (4.39 km^2) overlies the Arequipa Airport Ignimbrite. It is formed by two overlapping structures of low height, with two craters that lie below the surrounding ground level (Figure 4). The first emission center (crater I in Figure 4) has a cone basal diameter (Wco) of 640 m, the crater diameter (Wcr) reaches 360 m, and the average cone height (Hco) is 15 m, while the average flank slope is 6°. A basal deposit covering the ignimbrite is composed of scoria with mainly lapilli and scarce bombs (<1-m diameter), followed by a massive, unsorted, dark gray, and clast-supported (~70% blocks) deposit. The thickness of the ejecta ring is variable, with a major concentration in the southeastern flank.

The second emission center covers the northwestern half of the first crater, and is also partially covered on its northwestern edge by a blocky lava flow deposit (Uyu2) from the Chachani volcanic cluster (Uyupampa lava field; Aguilar et al., 2022). The Wco reaches 480 m, the Wcr is 320 m, the average Hco is 10 m, and the average flank slope is 10°. Lava flows and agglutinated scoria blocks form the rim of the crater (Figure 4). The base of the ejecta ring has moderately laminated layers of lapilli embedded in a whitish ash size matrix, overlain by a non-stratified deposit of dark red and black scoria blocks immersed in a medium to coarse brown ash matrix. The thickness of the uppermost scoria blocks deposit is irregular, and has its maximum value on the southwestern flank (~40 m). This last scoria deposit yielded a $^{40}Ar/^{39}Ar$ age of 97.7 ± 10.4 ka (Table 4). The floors of both craters are partially filled with fine sediments (sand and silt) suggesting the presence of water in the past. One km west of the craters, a ~20-m thick and dark-gray a'a lava flow crops out beneath tephra-fallout layers. The front and the upper surface of this lava flow is visible only along 120 m, making it difficult to determine the source vent. However, based on its proximity to the craters, the flow direction and the similarity in mineral content (mostly olivine phenocrysts) we assume that it was emitted from Ccapua volcano.

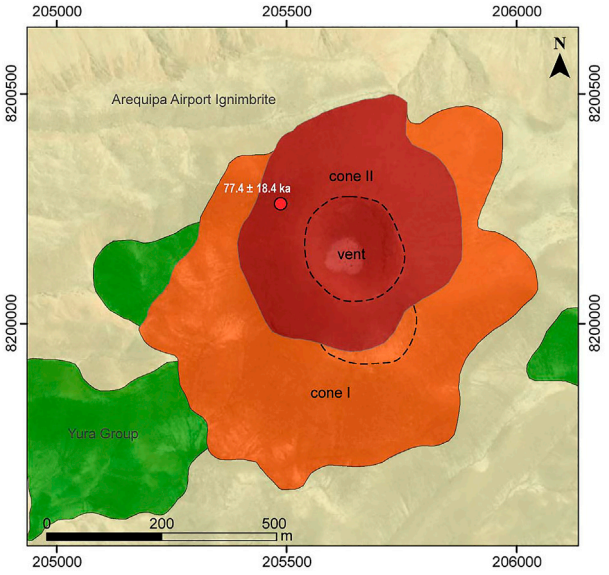

FIGURE 5
Geological map of Nicholson cone embedded on a Google Earth image.

In addition, a massive deposit of dark brown and black scoria blocks and bombs embedded in a fine matrix was emplaced following a southwestern direction, and reaches distances as far as 2 km. This deposit has a maximum thickness of 60 m at 1.2 km from the vent. Ballistic bread-crust bombs attributed to Ccapua, mantle the Arequipa Airport Ignimbrite in the surrounding areas at distances as far as 2 km.

4.1.3 Nicholson

Nicholson volcano (1.42 km^2) was built at the southwestern edge of the Yura Monogenetic Field on a plain formed by the ~1.65 Ma Arequipa Airport Ignimbrite (Paquereau-Lebti et al., 2008; Figure 5), which is cut by the Yura River to the east. The volcanic edifice consists of two superimposed scoria cones. The older cone has a mean Wco of 540 m, Wcr of 200 m, Hco of 90 m, and average flank slope of 28°. The younger cone is located in the northern part, and its cone morphology is characterized by semi-circular outlines, with a very well defined circular shape crater. This cone has a 520 m Wco, 210 m Wcr, 75-m Hco, and 26° average flank slope. Both cones were built by massive accumulations of black to dark red, poorly welded, unsorted, and clast-supported deposits, lacking any internal bedding. The constituents of these deposits are reddish and dark scoria clasts

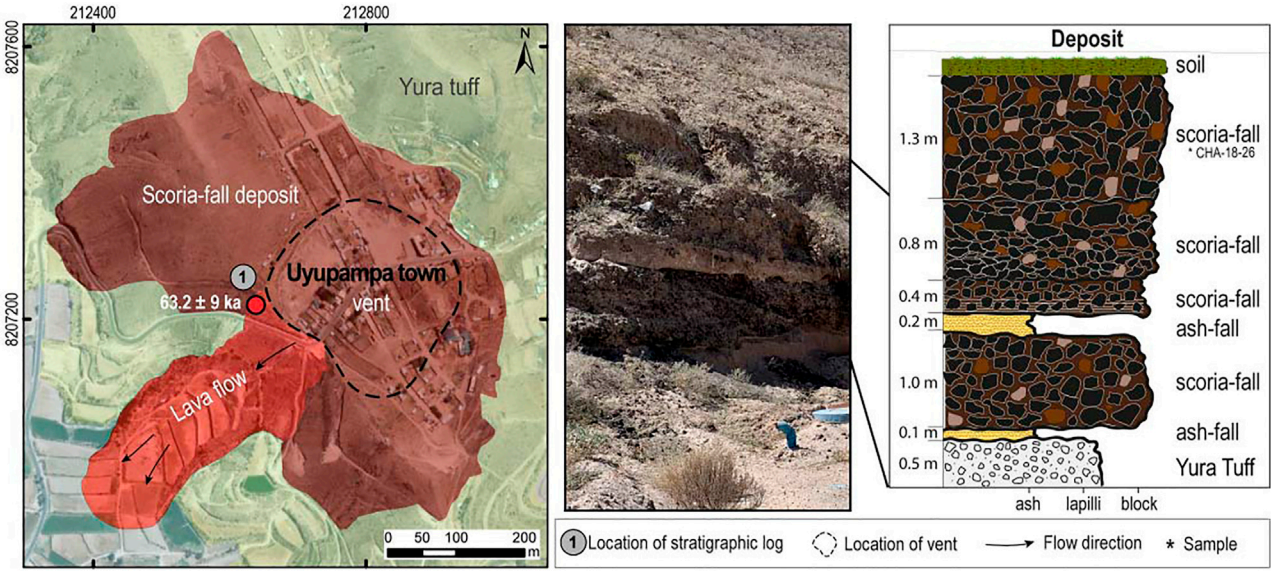

FIGURE 6
Geological map of Uyupampa volcano, showing a stratigraphic section and a picture of the outcrop where the section was described.

with lapilli to block sizes (<3-m diameter). Lava flow deposits border the northern and eastern side of the younger crater, while agglutinated blocks of scoria are found all around the crater rim. Ballistic fragments of ~30 cm can be found up to 900 m away from the vent. A scoria fall deposit of the younger cone was $^{40}Ar/^{39}Ar$ dated at 77.4 ± 18.4 ka (Table 4). In the lower part of the southeastern flank, 40–60 cm thick muddy and matrix-supported (50% of matrix) lahar deposits are observed, which incorporated angular scoria fragments (<10 cm in diameter). In most of its extension, Nicholson volcano is covered by a layer of reworked ash (~7–10 cm thick) from the 1600 B.P. eruption of Huaynaputina volcano, located 104 km to the southeast (e.g., Japura, 2018; Prival et al., 2020).

4.1.4 Uyupampa

Uyupampa volcano overlies the Yura Tuff, and its deposits cover 0.30 km^2. This volcanic center seems to be strongly eroded and its deposits were used as quarries for housing construction. However, a semicircular structure of ~300 m diameter is found in the present location of the town of Uyupampa, which may indicate the crater of the volcanic center. It is important to note that this monogenetic volcano is not related to the younger "Uyupampa lava-field" (blocky lavas) belonging to the Chachani Volcano Cluster (e.g., Aguilar et al., 2022) cropping out to the left side of La Paccha ravine (Figure 1).

The basal deposits of Uyupampa monogenetic volcano were emplaced over the Yura Tuff (Figure 6), and consist of pinkish ash layers (10–20 cm thick) interbedded with dark gray, moderately sorted scoria blocks/bombs - lapilli (35–130 cm thick) fallout deposits. At ~120 m east of the crater, pinkish ash-fall layers with scarce scoria fragments (<10 cm diameter) grade to unsorted, clast-supported, brown-black scoria block/bomb fallout deposits (up to 70 cm size and 95% blocks). These layers are overlain by diffusely laminated and dark gray scoria and lithic ash-lapilli layers. The upper units consist of an accumulation of unsorted, clast-supported, brown and black scoria block/bombs layers. Most of the pyroclastic deposits contain bread-crust and cauliflower texture bombs that reach up to 100 cm in diameter (at 300 m from the crater). Scoria bombs and other tephra fall deposits have quartz-sandstone and shale xenoliths and loose clasts (<30 cm).

The eruptive activity of this volcanic center culminated with the emplacement of a massive, olivine-rich a'a lava flow dated by $^{40}Ar/^{39}Ar$ method at 63.2 ± 9.0 ka (Table 4) which reached up to 500 m from the vent, following a southwest topographic low (Figure 6).

4.1.5 El Chiral

This volcanic unit was emplaced near the Ayo-Lluta-Arequipa Fault, covering 1.54 km^2. It is formed by a lobular-shaped lava dome (Figure 7), which is cut by a ~50-m thick and ~1.60 km long lava flow deposit. This lava flow fills a small NE-SW depression where volcanic deposits of the Tacaza Group and quartz sandstones (Hualhuani Formation) of the Yura Group crop out. The geoforms of the vent and lava bodies of El Chiral suggest a cylindrical shape conduit, and emplacement of the lava in a gently inclined topography (e.g., Murcia and Németh, 2020).

4.1.6 Patacocha

This eruptive center (~0.45 km^2) shows an irregularly shaped and complex edifice formed by two coalescing cones and three

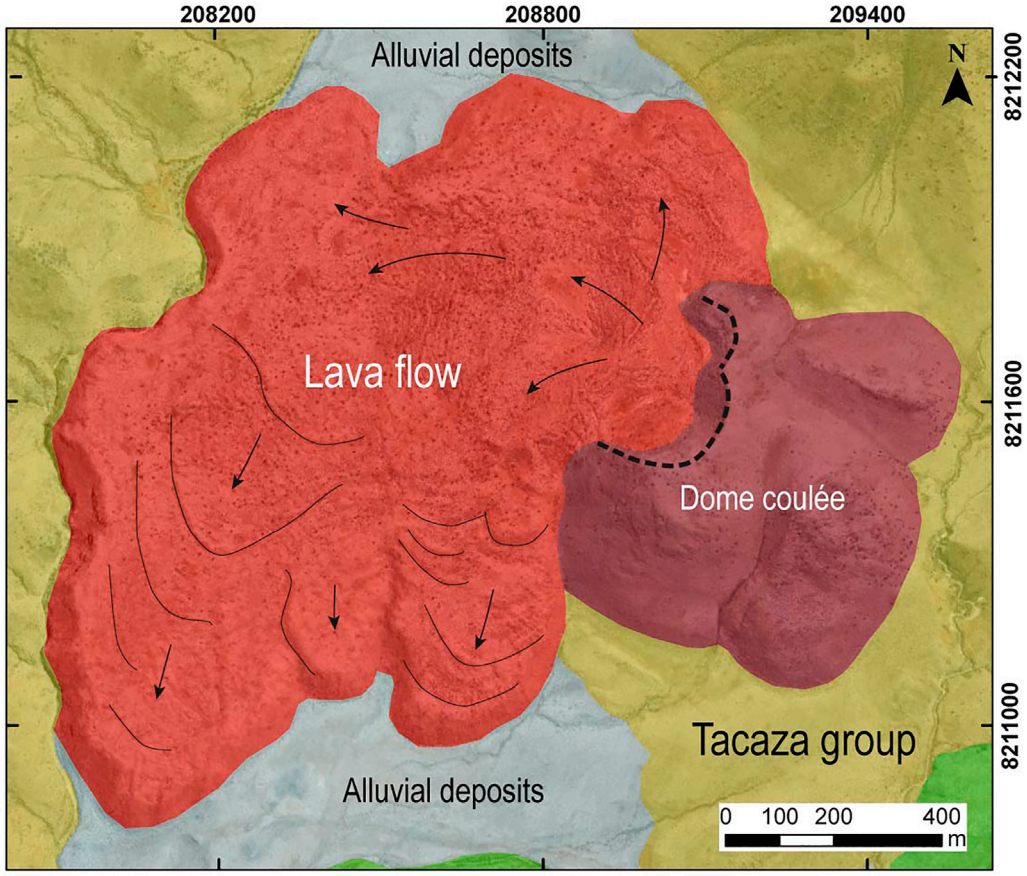

FIGURE 7
Geological map of El Chiral volcanic center, showing two units of dome coulée and lava flow deposits.

craters. The northwestern cone is capped by two coalescing craters (craters II and III), whereas the southeastern cone (crater I) has only one crater (Figure 8). Using Google Earth images and GIS software, we estimated the morphological parameters of the two cones: 1) Wco of 420 m, Wcr of 220 m, Hco of 24 m, and average flank slope of 14° for the northwestern cone. The smaller crater of 80-m diameter cuts the first larger crater. 2) Wco of 380 m, Wcr of 135 m, Hco of 40 m, and the average flank slope is 18° for the southeastern cone. The material expelled by this volcano covers deposits of the Tacaza Group, and apparently closed the channel of a stream, causing the damming of water and the formation of a lagoon called Patacocha (highland lagoon in Quechua). Due to the difficulty in accessing this area, it was not possible to take samples for laboratory analysis.

4.2 Volcano-structural setting

The local tectonic setting in which the Yura Monogenetic Field was emplaced consists of four groups of faults: N130°, N160°, N80° and N20°. This configuration is similar to the nearby Chachani volcano cluster described by Aguilar et al. (2022).

1) On satellite images, a N130° oriented lineament cuts the Potrero-Airport domes and coincides with the collapse scar of the middle unit of this group of domes (Aguilar et al., 2022). The N120°-130° faults extend to the east of the city of Arequipa and offset pyroclastic deposits at the base of El Misti volcano (Upper Pleistocene) in the Chiguata zone (Thouret et al., 2001). Another remarkable fault is the dextral and normal fault that cuts across the western flank of El Misti volcano (Thouret et al., 2001) and extends towards the east flank of Estribo stratovolcano with a N130° orientation.
2) At a regional scale, N120°-130° and N160° faults and lineaments display an *en-echelon* fault system, which extends to El Misti stratocone and Pichu-Pichu volcanic complex. In the eastern central part of the Chachani volcanic cluster, this system cuts these edifices. The orientation of these lineaments is probably controlled by perpendicular N80° faults.

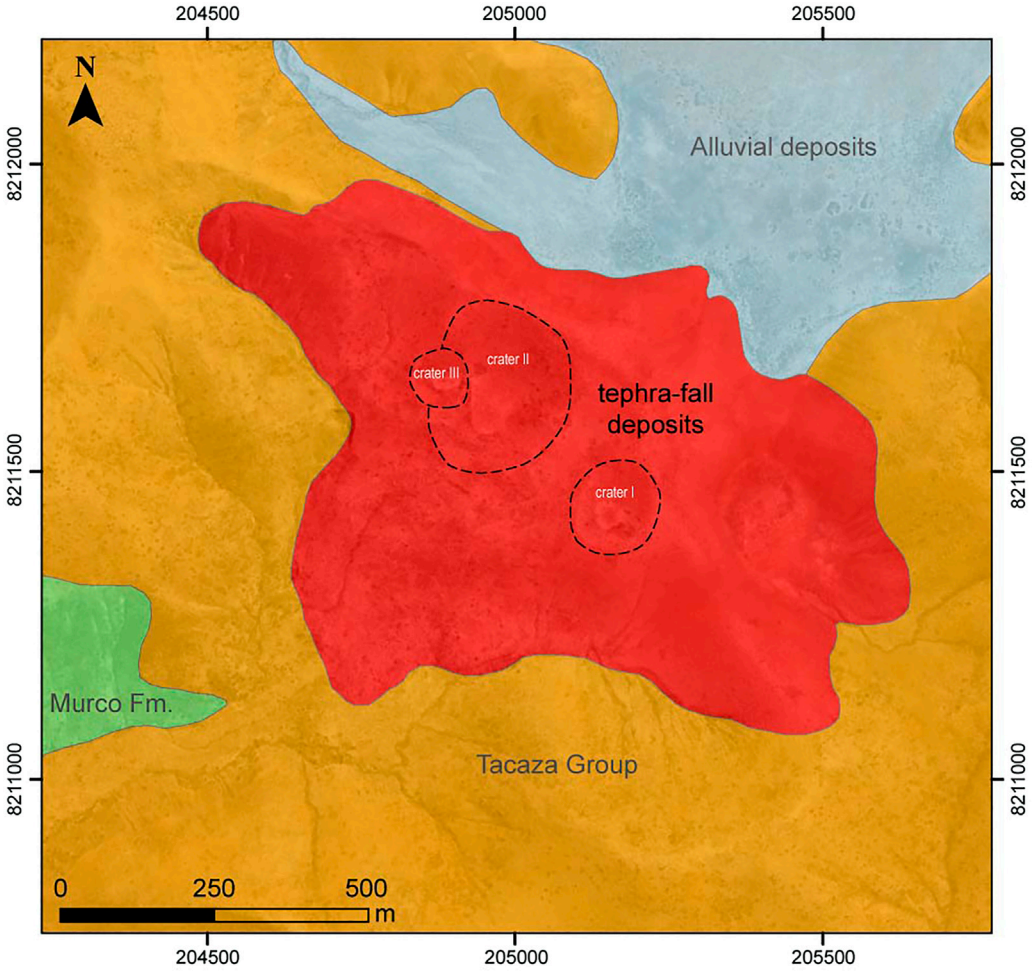

FIGURE 8
Geological map of Patacocha volcano, showing at least three identified vents.

3) A group of long faults and lineaments (~20 km), with a prevailing N80° direction, allow us to define a NE-SW structure which delimits the northwestern edge of the Arequipa basin (Mering et al., 1996; Thouret et al., 2001; Benavente et al., 2017). This fault intersects the Ayo-Lluta-Arequipa Fault (~N130° strike-slip and normal fault; Figure 1B).
4) Finally, the last group of short lineaments follows a N20-40° direction observed in the southern sector of the Chachani volcanic cluster. A remarkable feature in this area is the N20-40° predominant orientation of the majority of small eruptive vents, which have built the voluminous Airport-Potrero dome coulées. Uyupampa and Yura Viejo volcanoes in the Yura Monogenetic Field follow a similar trend.

The extensional zone along N80°- and N135°-trending faults is associated with fissures that allow the ascent of magmas to the surface (e.g., Huaman-Rodrigo et al., 1993). Magnetic measurement data for Nicholson volcano identified two E-W trending tabular bodies beneath the edifice, suggesting dyke-shaped feeding conduits (Rivera, 2021). E-W lineaments are also observed between Ccapua and Yura Viejo Volcanoes, and El Chiral and Patacocha volcanoes. Uyupampa and Yura Viejo volcanoes are aligned following a N40° trend. In the southwestern flank of Chachani, several small vents are also aligned along N10° and N40° eruptive fissures (Aguilar et al., 2022).

The N130° and N80° structures that we identified in the Yura Monogenetic Field and Chachani Volcano Cluster resemble those described by Huaman-Rodrigo et al. (1993) in the region of the Río Colca - Nevado Ampato-Sabancaya volcano, located about 50 km northwest of Yura (Maca and Huambo faults). In the area near Huambo NW of Yura, and in the northern flank of Chachani Volcano Cluster, N80° normal faults (Huaman-Rodrigo et al., 1993; Sempere and Jacay, 2006; Aguilar et al., 2022) are considered active because they cut recent

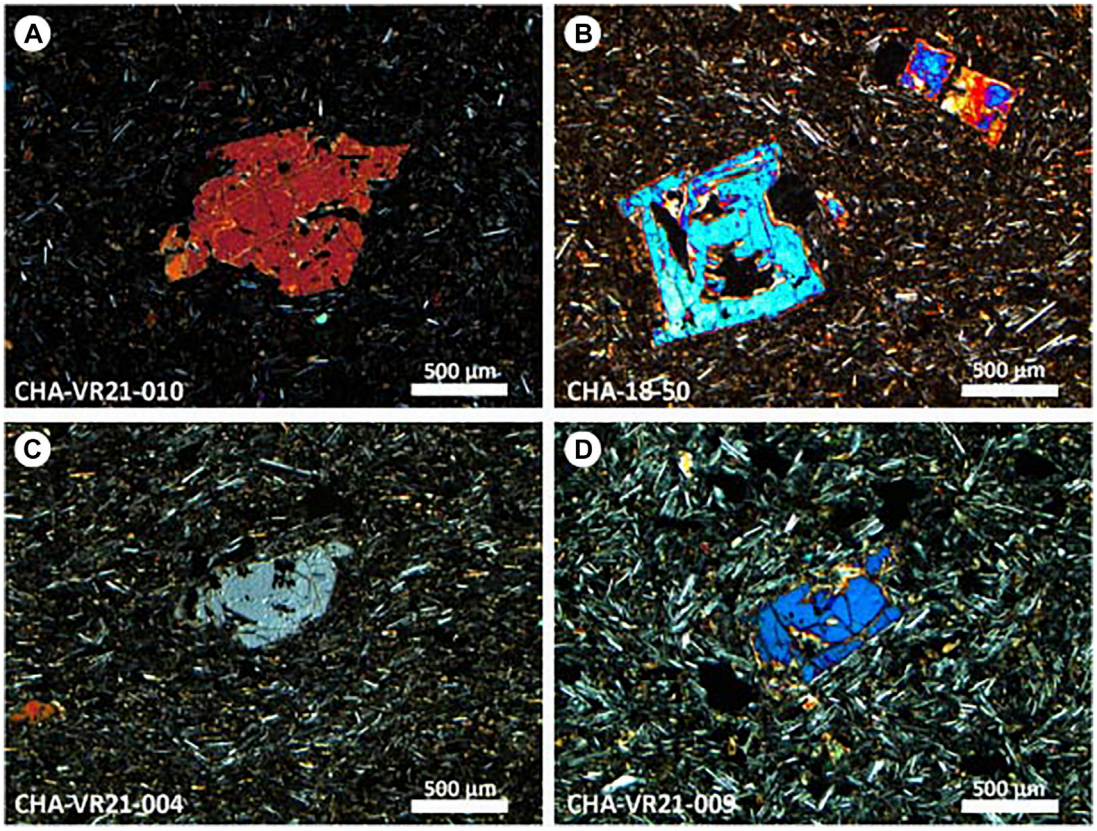

FIGURE 9
Observed textures in thin sections of the Yura monogenetic volcanoes. Olivine phenocryst is a ubiquitous mineral phase in all analyzed samples. **(A)** Subhedral olivine phenocryst in microlithic groundmass from Nicholson cone; **(B)** Skeletal texture observed in olivine in sample from Ccapua volcano; **(C)** Olivine phenocryst in microlithic groundmass in Yura Viejo volcano rocks; **(D)** Subhedral olivine phenocryst in Uyupampa lavas.

Late Pleistocene lava flows and Holocene colluvial deposits. A destructive earthquake took place on one of them at Maca, on the left bank of the Río Colca canyon in 1992 (e.g., Antayhua et al., 2001). Other similar events occurred in August 2016 and March 2022, damaging houses and infrastructure.

5 Petrography and geochemistry

5.1 Modal mineralogy

The mineral content of all analyzed samples from the volcanic centers of Yura Monogenetic Field is similar (Figure 9 and Table 2). All analyzed samples are porphyritic (7–10 vol%) and vesicular. In all samples, the dominant mineral is olivine, while the groundmass contains ortho- and clinopyroxene, plagioclase and glass.

Olivine (7–10 vol%; ≤2 mm) occurs as subhedral phenocrysts with subrounded and embayed edges. In some cases, it has skeletal and breakdown textures (Figure 9). Pyroxene is present only in the groundmass (20–42 vol%; <400 µm; clinopyroxene > orthopyroxene) together with plagioclase microlites (26–53 vol %; <300 µm), giving the matrix a pilotaxitic texture by almost all samples (Table 2). Volcanic glass (<5 vol%) is found encompassing the microlites. The opaque minerals (<5 vol%; <800 µm) present anhedral and subhedral forms, and occur as accessory minerals as inclusions in olivine, or as replacement in crystal molds and disseminated in the groundmass (Table 2). The vesicles (5–29 vol %) have irregular shapes.

5.2 Whole-rock major and trace element chemistry

Analyzed samples are given in Table 3. The scoria and lavas consist of high-K (1.60–2.01 wt% K_2O) calc-alkaline rocks, which is a typical characteristic of the modern volcanic arcs in the Central Volcanic Zone (e.g., Wilson, 1986). Basaltic-andesite is an ubiquitous composition throughout the entire volcanic field, ranging from 50.9 to 55.6 wt% SiO_2 (Peccerillo and Taylor, 1976;

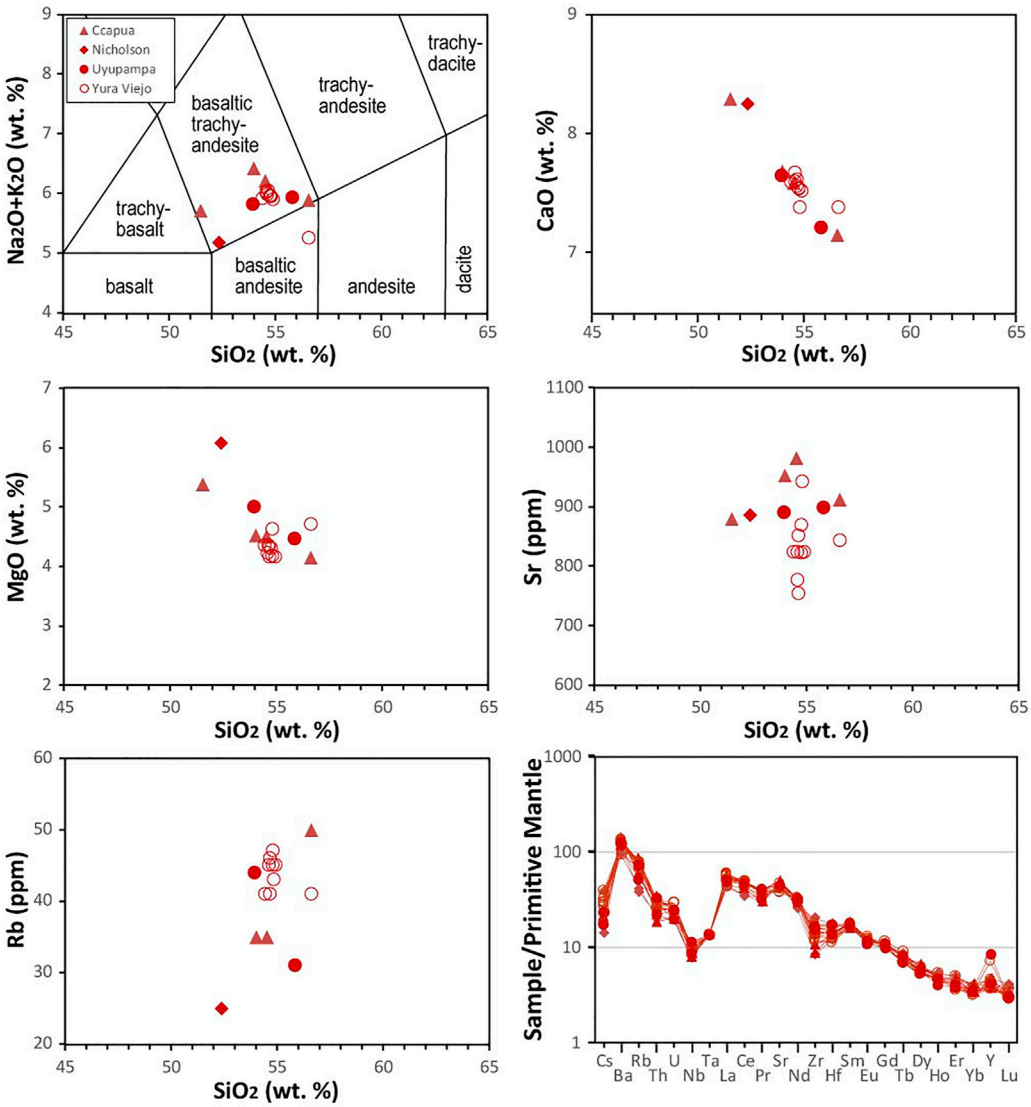

FIGURE 10
Chemical composition of Yura monogenetic volcanoes. Total Alkali-Silica versus SiO_2 diagram (Le Bas et al., 1986) showing the classification of Nicholson, Ccapua, Yura Viejo and Uyupampa volcanoes. Major oxides are shown as recalculated volatile-free values. Ca, MgO, Sr, and Rb versus SiO_2 diagrams show the compositional variation. Multi-element diagrams normalized to primitive mantle (Sun and McDonough, 1989) showing trace element patterns of rock samples.

Figure 10). The least differentiated olivine-rich samples are found in the Ccapua and Nicholson volcanic centers. In Harker diagrams, some of which are shown in Figure 10, MgO, CaO, Fe_2O_3 contents show negative correlation with SiO_2 indicating a common differentiation trend. Similarly, transition elements (e.g., Ni, Cr, V) and Dy are negatively correlated to SiO_2 suggesting that fractional crystallization is the major differentiation process in these magmas. Most incompatible elements such as Rb, U and Th together with Sm are positively correlated with increasing SiO_2.

A multi-element diagram normalized to primitive mantle (Sun and McDonough, 1989; Figure 10) displays a similar pattern for all analyzed samples: enrichment in LILE (Cs, Rb, Ba, Sr) relative to HFSE (Nb, Ta). The patterns for scoria and lavas from Yura Monogenetic Field are similar to those observed for other monogenetic volcanoes in the region such as Andahua-Huambo-Orcopampa (e.g., Delacour et al., 2007; Mamani et al., 2010; Galas, 2011) and for Central Volcanic Zone rocks (e.g., Wilson, 1986; Davidson et al., 1991; Stern, 2004).

TABLE 5 Summary of characteristics and morphologic parameter for volcanic centers in the Yura Monogenetic Field.

Volcano name	Volcano-sedimentary process	Typical deposits	Morphology parameters					Observations	Eruption style	Classification
			Wco (m)	Wcr (m)	Hco (m)	Wcr/Wco	Hco/Wco			
Nicholson	Proximal fallout and ballistics, rootless lava flow	Ash to block accumulation in the flanks, tephra blanket in the distal areas	Cone I: 616 Cone II: 520	200 210	90 75	0.32 0.40	0.15 0.14	vent migration	Strombolian	Scoria cone
Ccapua	Fallout from eruptive column, PDC, lava flow, ballistics	Ash to block/bomb, agglutinated scoria in the ejecta ring	Crater I: 640 Crater II: 480	360 320	~15 ~10	0.56 0.67	0.02 0.02	vent migration, crater filled with post-eruption sediments	Phreatomagmatic - Strombolian	Maar
Yura Viejo	Fallout from eruptive column, PDC, ballistics. Lava flow, lahar flow	Ash to block/bomb beds in the ejecta ring, tephra blanket in distal areas	~800	520	~25	0.65	0.03	lava infill the crater, relief inversion. Crater below the surrounding surface	Phreatomagmatic - Strombolian	Maar (?)
Uyupampa	Fallout from eruptive column, PDC, ballistics. Lava flow	Ash to block/bomb beds in the ejecta ring, bread-crust and cauliflower bombs	~510	~300	-	-	-	tephra blanket in distal areas	Phreatomagmatic - Strombolian	Tuff ring/ Maar (?)
Patacocha	Fallout from eruptive column (?)	Tephra fallout	Cone I: 380 Cone II: 420	135 220	~40 ~24	0.36 0.52	0.11 0.05	accumulation of tephra dammed the ravine forming the Patacocha lagoon	no information	Scoria cone
El Chiral	lava flow	Lava rock	Dome coulée: length: 420 m, width: 265 m, thickness: ~105 m Lava flow: length: 1600 m, thickness ~50						Effusive	Dome coulée and lava flow

Wco, cone basal diameter; **Wcr**, crater diameter; **Hco**, cone height.

6 Discussion

6.1 Eruptive style and classification of volcanoes in the yura monogenetic field

At monogenetic volcanoes, the internal magma dynamics that occurs at shallow depths and the characteristics (form and dimension) of the conduit are linked to the way that magma is released at the surface, and the volcanic edifice construction (Murcia and Németh, 2020, and references therein). The topography where the magma is deposited also plays a role in the geoform of the volcano. The eruptive activity forming the monogenetic volcanoes usually consist of magmatic or phreatomagmatic explosions and in many cases accompanied by effusive emissions (Németh and Kereszturi, 2015). Field observations and description of the deposits in the Yura Monogenetic Field allow us to suggest: 1) Nicholson (and probably Patacocha) volcanoes were built by Strombolian (magmatic) eruptions. 2) Ccapua, Yura Viejo and Uyupampa volcanoes show ash to block particle sizes embedded in a muddy matrix, which suggests the interaction between magma and water, generating phreatomagmatic eruptions. However, accumulation of mainly scoria blocks/bombs and lava flows suggests Strombolian eruption phases. 3) El Chiral is composed of lava flows and coulées. Due to the lack of field data, it is not possible to characterize the type of eruption, although it was probably mainly effusive.

Basic measurements of morphometric parameters such as the cone basal diameter (Wco), crater diameter (Wcr) and cone height (Hco) allow obtaining morphometric signatures for classification of monogenetic volcanoes (e.g., Wood, 1979; Németh and Kereszturi, 2015). This classification includes spatter cones (Wco = 0.08 km, Wcr/Wco = 0.36 km and Hco/Wco = 0.22 km), scoria/cinder cones (Wco = 0.8 km, Wcr/Wco = 0.4 km and Hco/Wco = 0.18 km), as well as maars and tuff rings (Wco = 1.38 km, Wcr/Wco = 0.6 km and Hco/Wco = 0.02 km) from average dimensions (Wood, 1979). Based on characterization parameters described by Németh and

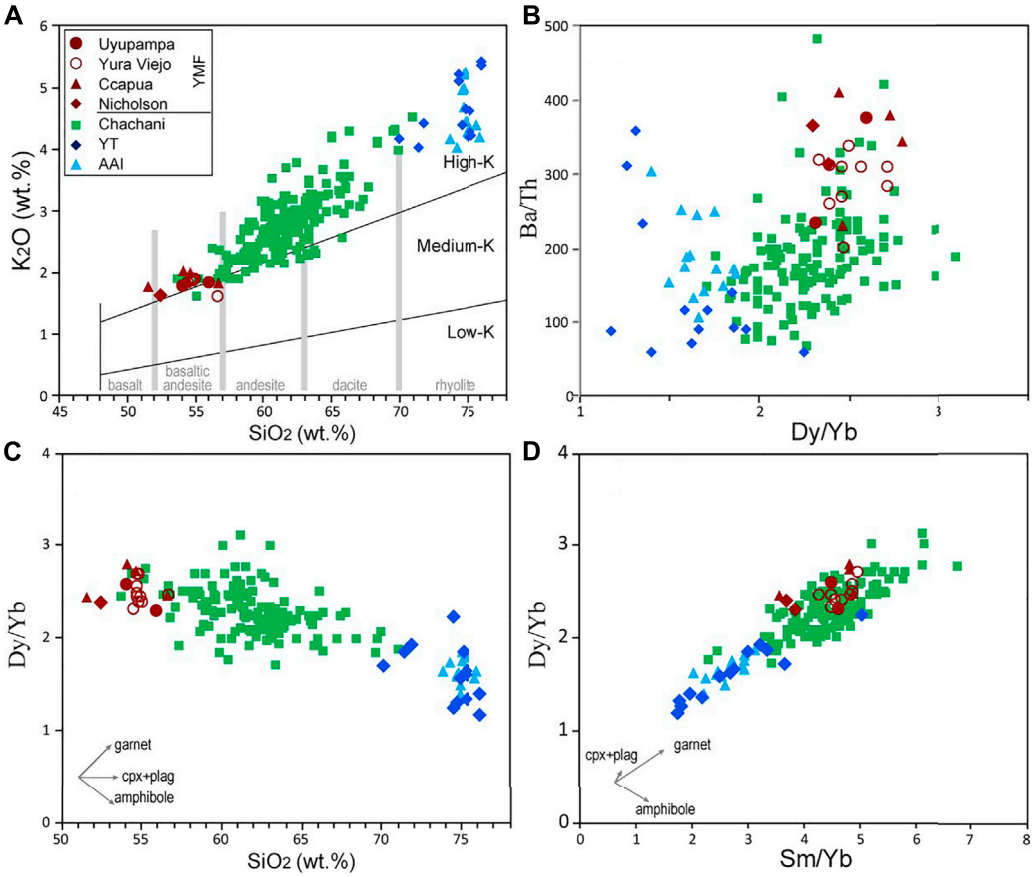

FIGURE 11
SiO_2 versus K_2O diagram (after Peccerillo and Taylor, 1976; **(A)**, and trace element signatures **(B, C, D)** in the Yura Monogenetic Field rocks for the purpose of comparison with available datasets of nearby Yura Tuff, Arequipa Airport Ignimbrite and Chachani volcanic Cluster (Paquereau-Lebti et al., 2006; Mamani et al., 2010; Aguilar et al., 2022). The inset trends of evolution in **(C)** and **(D)** were taken from Wörner et al. (2018). Cpx: clinopyroxene, plag: plagioclase.

Kereszturi (2015), and Wood (1979), we suggest that the eruptive activity in the study area produced scoria cones (Nicholson and Patacocha), maars (Ccapua, Yura Viejo and Uyupampa), and a dome coulée and lava flow (El Chiral). A summary of the main characteristics and morphologic parameters is presented in Table 5.

6.2 Chemical comparison with surrounding volcanoes

Figure 11 shows the comparison of Yura Monogenetic Field with surrounding Pleistocene volcanic rocks. Major element oxides show similar patterns among Yura Field, Chachani cluster, Yura Tuff and Arequipa Airport Ignimbrite. The Yura Field samples are the least differentiated magmas in the Arequipa basin; only some lava and scoria samples from the Chachani cluster exhibit similar composition. The Chachani volcanic cluster shows an intermediate and wider compositional range from basaltic andesite to rhyolite (54–71 SiO_2 wt%). The most differentiated samples belong to the Arequipa Airport Ignimbrite, which has a homogeneous silica content (74–76 SiO_2 wt%; Paquereau-Lebti et al., 2006). The Yura Tuff also shows highly differentiated compositions, but with a less homogeneous silica content (70–76 SiO_2 wt%).

Incompatible-element ratios such as Ba/Th vs. Dy/Yb and Dy/Y vs. Sm/Yb (Figure 11) exhibit overlapping fields with higher values in Ba/Th and Dy/Yb in the Yura Monogenetic Field and Chachani cluster. By contrast, the more evolved magmas of Arequipa Airport Ignimbrite and Yura Tuff show lower Dy/Yb and Sm/Yb values.

Due to the proximity of their sources, magmas generating the ignimbrites, the Chachani cluster and the Yura Monogenetic Field, could have a similar source and have passed through a similar substrate in their way to the surface, so they would have similar contaminants (e.g., sedimentary rocks of the Yura

Group). However, the abundance of xenoliths and subangular bedrock fragments found in the Yura Monogenetic Field deposits indicate that the assimilation process was much less effective in them. These monogenetic rocks and less differentiated lavas from Chachani cluster show similar basaltic-andesite compositional patterns (Figure 11). In general, rocks from the Yura Monogenetic Field may represent the mafic end-member of the Pleistocene-Holocene volcanic products in the Arequipa basin and surrounding areas (e.g., Aguilar et al., 2022). At a regional scale, these magmas show one of the least differentiated magmas in the Central Volcanic Zone (e.g., Delacour et al., 2007; Mamani et al., 2010; Torres et al., 2020).

6.3 Chronology of monogenetic volcanism in the yura valley

Magmatic activity in the Arequipa region occurred continuously during the Pleistocene. The Arequipa Airport Ignimbrite marks a moderate to large magnitude explosive event (~18 km^3) that occurred *c.* 1.65 Ma (Paquereau-Lebti et al., 2006). This event emplaced pyroclastic density currents that filled the Arequipa depression, and caused the formation of a possible caldera (García et al., 1997). The geographic location of the ignimbrite source is likely covered by the edifices composing the Chachani volcano cluster (Paquereau-Lebti et al., 2006, 2008; Aguilar et al., 2022). After caldera formation, andesitic lava flows were emplaced in the western edge of Chachani, with outcrops now located in the Quebrada La Paccha (Figure 1). Yura Tuff (*c.* 1.28 Ma; Paquereau-Lebti et al., 2006) overlies those lavas and fills the Yura valley (formed between the current northwestern side of Chachani and the wall formed by Yura Group units; Figure 1). The Chachani volcanic cluster started its activity at ~1.01 Ma on the northeastern side, having recorded continuous activity until *c.* 641.8 ka with a possible hiatus that lasted until *c.* 463 ka. After *c.* 463 ka, the eruptive activity migrated to the central and southern part of the whole cluster (Aguilar et al., 2022). Towards the lower western flank of Chachani volcanic cluster and covering ignimbrite deposits, the Uyupampa lava field is composed of porphyritic lava flows, one of which yield an age of *c.* 232 ka. The youngest dated rock in the Chachani Volcanic Cluster belong to a block-and-ash deposit from Cabreria dome (*c.* 56.5 ka; Aguilar et al., 2022).

The oldest lithological units, on which the volcanoes of the Yura Monogenetic Field (e.g., El Chiral and Patacocha) were emplaced, belong to the Tacaza Group (*c.* 30–24 Ma; e.g., Mamani et al., 2010) in the northwestern sector of the field. However, the degree of preservation of volcanic structures such as the craters (cones), lobes and ridges (lava flows) suggests that Patacocha and El Chiral are much younger than c. 24 Ma. The ages obtained for the Yura Viejo, Ccapua, Nicholson and Uyupampa volcanoes match the stratigraphy of the area since they cover older deposits of the Arequipa Airport Ignimbrite and the Yura Tuff. The *c.* 168 ka age of Yura Viejo is in accordance with the degree of preservation of its deposits. Nicholson and Ccapua volcanoes were built over deposits of the Arequipa Airport Ignimbrite, while the Uyupampa and Yura Viejo volcanoes directly overlie the Yura Tuff. Based on the degree of preservation of the Patacocha scoria cones and El Chiral lava flow-dome coulée, we suggest that these volcanoes are relatively contemporaneous to the dated ones. Thus, the Yura Monogenetic Field would have been active in a time window of 141 kyr, between *c.* 195 ka and *c.* 54 ka. We note that this range of ages is younger than expected since the second crater of Ccapua volcano was partially covered by a lava flow from the Uyupampa field (Chachani volcanic cluster, Figure 1). Detailed fieldwork however, allowed us to determine that Ccapua was formed after the emplacement of the lava flow (Uyu1) dated by $^{40}Ar/^{39}Ar$ at 231.7 ± 36.2 (on groundmass; Aguilar et al., 2022), and was later covered by another lava flow (Uyu2) which should be younger than 97.7 ± 10.4 ka. The new ages obtained allow us to suggest that the eruptive activity of the Yura Monogenetic Field temporally coincided with the youngest edifices of Chachani volcanic cluster (Aguilar et al., 2022) and the basal units of the Misti composite cone (≤112 ka; Thouret et al., 2001). Future radiometric dating of the volcanic products from Patacocha and El Chiral are necessary to better constrain the age and duration of the magmatism in this monogenetic field.

6.4 Yura monogenetic field as potential geosite for education and awareness of volcanic hazards

Recent volcanic activity in southern Peru has caused significant impacts to the population and economic activity for the communities settled in surrounding areas. Recent volcanic eruptions of the Ubinas volcano (2006–2009, 2014–2017 and 2019) have affected agriculture, critical infrastructure, and forced authorities to evacuate the people to shelters in safe areas (e.g., Rivera et al., 2010). The Sabancaya volcano began a new long-lasting vulcanian eruption process in 2016, and continues to this day, with no signs of ending in the near future. The ash emitted by frequent explosions of Sabancaya have caused damage to agriculture, livestock, and has even affected air traffic in the city of Arequipa (e.g., Aguilar, 2019; INGEMMET, 2021). In addition, during rainy seasons, the occurrence of lahars in the ravines that descend from the Misti and Chachani volcanoes has caused the destruction of homes, damage to basic infrastructure, and casualties (e.g., Rivera et al., 2018). These events remind us that volcanic eruptions and associated processes can negatively impact the development of communities; therefore, it is necessary that the population

and decision-makers develop measures to reduce the impact of these hazards. According to the record of eruptive activity, the hazards related to monogenetic volcanoes in the Yura Monogenetic Field are tephra-fall, ballistic fall, scoria flow, lava flow and lahar. Thus, the study of structures and deposits of the Yura Monogenetic Field can allow the identification of potential geosites for scientific, educational and geoturism uses and related to volcanic hazards. Nicholson is an easily accessible volcano to explain Strombolian eruptions and the formation of scoria cones. Ccapua volcano clearly shows the superposition of two craters and the formation of a maar which is partially covered by a younger lava flow. The Yura Viejo volcano shows explosive Strombolian-type activity combined with lahar flows, culminating with the emplacement of a lava flow. In addition, outcrops of ignimbrites that represent violent explosive eruptions can be seen in the area, as well as very representative sequences of sedimentary rocks of the Yura Group. The small monogenetic volcanoes also provide superb views of the surrounding larger volcanoes, and this, combined with their accessible outcrops and clear geology, provides an especially rich educational and geotouristic resource. This is especially important for communicating and understanding hazards and risk, as the urban centers and human infrastructure are visible in the landscape. In recently published press releases, it was indicated that the town of Yura Viejo is located in the crater of an extinct monogenetic volcano. This information was well-received by the local inhabitants and has attracted the attention of visitors, whose flow is increasing, not only to Yura Viejo, but also to the nearby Ccapua waterfalls (La Paccha ravine near Ccapua maar; Figure 1).

Due to its proximity to the urban area of Arequipa, and the good preservation of its deposits, the Yura Monogenetic Field has a great potential to promote geotourism for recreational, scientific and educational purposes in the face of the volcanic hazards (e.g., Galas et al., 2018; Arias et al., 2021). The valorization of these geosites could help in the popularization of these places and above all in their preservation by using an information simple to understand. There are examples of monogenetic fields that are growing tourist attractions, such as the Andagua monogenetic volcanoes (e.g. Galas et al., 2018), which are located within the Peruvian "Colca and Andagua Volcanoes" UNESCO Global Geopark. Other geosites are La Garrotxa monogenetic field in Spain (e.g., Planagumà-Guàrdia et al., 2022), and the Chaine de Puys in Clermont-Ferrand, France (e.g. Vereb et al., 2020).

7 Concluding remarks

The study of the eruptive history of monogenetic volcanic centers is useful to define the sequence of events and the dynamics of the eruptions that built these volcanic edifices. Such volcanoes are key for understanding the geological evolution of an area, as they reflect the magma dynamics, the tectonics and the subsequent surface processes. Therefore, the combination of volcanic stratigraphy, geochemical and petrographic studies of volcanic activity in the Yura Monogenetic Field is important to better understand the evolution of volcanism in southern Peru. The study of the deposits has allowed us to reconstruct the history of this monogenetic field emplaced after medium-size ignimbrites formation in the Arequipa tectonic depression. Our new data suggest that volcanism in the Yura Monogenetic Field was active between *c.* 195 ka and *c.* 54 ka, which is more recent than previously expected (*c.* 1278 ka–*c.* 232 ka). The stratigraphic position and the degree of preservation of cone craters, lobes and ridges in lava flow/coulées indicate that El Chiral and Patacocha are much younger than Tacaza Group (Oligocene) as they cover volcanic units assigned to this group (Figure 1). However, due to their geographical proximity, similarity in their petrographic and chemical characteristics these volcanoes are contemporaneous to the dated ones. Hence, the volcanism in the area lasted for ~141 ka, beginning with the Yura Viejo volcano and probably finishing with Uyupampa volcano.

Bulk-rock major and trace elements highlight the fact that compositions have not varied with the locations of vents along the monogenetic field. These volcanic centers have relatively homogeneous basaltic-andesite compositions (50.9–55.6 wt% SiO_2), being among the least differentiated Quaternary rocks in the surrounding areas of the Arequipa basin. The dynamic of eruptions is marked by Strombolian and phreatomagmatic explosive activity, combined with scattered lava flows and small pyroclastic density current deposits (scoria flows). In most of the volcanoes, scoria flows including glassy bread-crust and cauliflower bombs suggest phreatomagmatic activity that crop out together with lahar deposits.

The Yura Viejo volcano shows one of the most complex histories in the Yura Monogenetic Field. The observed deposits indicate that its activity began with phreatomagmatic evolving to Strombolian eruptions, which expelled rock fragments (tephra) up to 1 km away from the crater. Subsequently, it generated a lava flow that was emplaced in a small gorge reaching a distance of ~1 km towards the current Yura River, ending its eruptive activity.

This contribution has revealed the presence of a monogenetic field in the northwestern edge of the Arequipa basin by locating, studying and dating unknown volcanic centers. The results obtained provide important information to improve the knowledge of recent volcanic activity in the Arequipa region, which is relevant for volcanic hazard assessment and related risk management. This information could be also useful for the knowledge of the territory and identification of geosites, promote their conservation and propose new areas for education about geohazards and risk.

Data availability statement

The original contributions presented in the study are included in the article/Supplementary Material, further inquiries can be directed to the corresponding author.

Author contributions

RA, DA and NM worked in the conception, design of the study, and drafted the original manuscript. The first three authors together with BV, carried out the fieldwork and mapping. KC and ET worked in photogrammetry for high-resolution images. HG and VS prepared the samples, analyzed and drafted the $^{40}Ar/^{39}Ar$ data. All authors reviewed the manuscript.

Acknowledgments

We thank the editor, S. Guzman, reviewers K. Németh and Dario Pedrazzi for their comments and constructive suggestions made on the early version of the manuscript, which helped to improve its content. This work stems from the research studies developed by Instituto Geológico Minero y Metalúrgico (INGEMMET) through the project "GA-17D: Estudio de peligros del Complejo Volcánico Chachani". The work was carried out within the framework of UNESCO - IGCP 692 Project: Geoheritage for Geohazard Resilience Project. Fieldwork of BV was supported by the Agence Nationale de la Recherche of the French government through the program Investissements d'Avenir (16-IDEX-0001 CAP 20-25). We thank the staff of the analytical chemistry and sample preparation units of the INGEMMET laboratories. T. Flaherty is also acknowledged for the English improvement of a previous version of the text.

Conflict of interest

The authors declare that the research was conducted in the absence of any commercial or financial relationships that could be construed as a potential conflict of interest.

Publisher's note

All claims expressed in this article are solely those of the authors and do not necessarily represent those of their affiliated organizations, or those of the publisher, the editors and the reviewers. Any product that may be evaluated in this article, or claim that may be made by its manufacturer, is not guaranteed or endorsed by the publisher.

Supplementary material

The Supplementary Material for this article can be found online at: https://www.frontiersin.org/articles/10.3389/feart.2022.904914/full#supplementary-material

References

Acocella, V., Salvini, F., Funiciello, R., and Faccenna, C. (1999). The role of transfer structures on volcanic activity at Campi Flegrei (Southern Italy). *J. Volcanol. Geotherm. Res.* 91 (2–4), 123–139. doi:10.1016/s0377-0273(99)00032-3

Acosta, H., Mamani, M., Alvan, A., Oviedo, M., and Rodriguez, J. (2010). "Actividad tectónica del sistema de fallas Incapuquio durante la formación de la cuenca Arequipa en el Jurásico". *XV congreso peruano de Geología. CD Resúmenes extendidos.*

Aguilar, R. (2019). "Exposure-based risk assessment of tephra-fall associated with long-lasting Vulcanian eruptions at Sabancaya volcano, Peru," in *These de Specialisation in the assessment and management of geological and climate related risk - cerg-C 2018* (Geneva: University of Geneva).

Aguilar, R., Thouret, J.-C., Samamniego, P., Wörner, G., Jicha, B., Paquette, J.-L., et al. (2022). Growth and evolution of long-lived, large volcanic clusters in the central Andes: The Chachani Volcano cluster, southern Peru. *J. Volcanol. Geotherm. Res.* 426, 107539. doi:10.1016/j.jvolgeores.2022.107539

Alván, A., Jacay, J., Caracciolo, L., Sánchez, E., and Trinidad, I. (2018). Sedimentary facies analysis of the Mesozoic clastic rocks in Southern Peru (Tacna, 18°S): Towards a paleoenvironmental Redefinition and stratigraphic Reorganization. *J. S. Am. Earth Sci.* 84, 399–421. doi:10.1016/j.jsames.2018.04.014

Antayhua, Y., Tavera, H., and Bernal, I. (2001). Análisis de la actividad sísmica en la región del volcán Sabancaya (Arequipa). *Bol. Soc. Geol. Perú* 92, 78–79.

Arias, C., Manrique, N., Aguilar, R., and van Wyk de Vries, B. (2021). "Geosite assessment in Arequipa city - Peru: UNESCO IGCP 692 project 'geoheritage for geohazard resilience," in The 23rd EGU General Assembly.

Armijo, R., Lacassin, R., Coudurier-Curveur, A., and Carrizo, D. (2015). Coupled tectonic evolution of Andean orogeny and global climate. *Earth. Sci. Rev.* 143, 1–35. doi:10.1016/j.earscirev.2015.01.005

Benavente, C., Delgado, F., García, B., Aguirre, E., and Audin, L. (2017). Neotectónica, Evolución y Peligro Sísmico en la Región Arequipa. *INGEMMET, Bol. Ser. Geodinámica Ing. Geol. N°* 64, 395.

Benavides, V. (1962). Estratigrafía pre-terciaria de la Región de Arequipa. *Bol. Soc. Geol. del Perú, Tomo* XXXVI, 58.

Callot, P., Sempere, T., Odonne, F., and Robert, E. (2008). Giant submarine collapse of a carbonate platform at the Turonian-Coniacian transition: The Ayabacas Formation, southern Peru. *Basin Res.* 20 (3), 333–357. doi:10.1111/j.1365-2117.2008.00358.x

Carlotto, V., Quispe, J., Acosta, H., Rodríguez, R., Romero, D., Cerpa, L., et al. (2009). Dominios geotectónicos y metalogénesis del Perú. *Bol. Soc. Geol. Perú* 103, 1–89.

Condit, C. D., and Connor, C. B. (1996). Recurrence rates of volcanism in basaltic volcanic field: An example from the Springerville volcanic field, Arizona. *Geol. Soc. Am. Bull.* 108, 1225–1241. doi:10.1130/0016-7606(1996)108<1225:rrovib>2.3.co;2

Connor, C. B., and Conway, F. M. (2000). "Basaltic volcanic fields," in *Encyclopedia of volcanoes: San diego*. Editor H. Sigurdsson (Academic Press), 331–343.

Connor, C. B., Stamatakos, J. A., Ferrill, D. A., Hill, B. E., Ofoegbu, G. I., Conway, F. M., et al. (2000). Geologic factors controlling patterns of small-volume basaltic volcanism: Application to a volcanic hazards assessment at Yucca Mountain, Nevada. *J. Geophys. Res.* 105, 417–432. doi:10.1029/1999JB900353

Davidson, J. P., Harmon, R. S., and Wörner, G. (1991). "The source of Central Andean magmas; some considerations," in *Andean magmatism and its tectonic*

setting geol soc amer spec paper. Editors R. S. Harmon and C. W. Rapela, 265, 233–244.

Delacour, A., Gerbe, M.-C., Thouret, J.-C., Wörner, G., and Paquereau, P. (2007). Magma evolution of quaternary minor volcanic centres in southern Peru, central Andes. *Bull. Volcanol.* 69 (6), 581–608. doi:10.1007/s00445-006-0096-z

Diefenbach, A., Crider, J., Schilling, S., and Dzurisin, D. (2012). Rapid, low-cost photogrammetry to monitor volcanic eruptions: An example from mount st. Helens, Washington, USA. *Bull. Volcanol.*, 74. 579–587. doi:10.1007/s00445-011-0548-y

Galas, A., Paulo, A., Gaidzik, K., Zavala, B., Kalicki, T., Churata, D., et al. (2018). Geosites and geotouristic attractions proposed for the project geopark Colca and volcanoes of Andagua, Peru. *Geoheritage* 10 (4), 707–729. doi:10.1007/s12371-018-0307-y

Galas, A. (2011). The extent and volcanic structures of the Quaternary Andahua Group, Andes, southern Peru. *Ann. Soc. Geol. Pol.* 81, 1–19.

García, F., Chorowicz, J., and Legros, F. (1997). La caldera Chachani, gran centro explosivo plioceno-holoceno del sur del perú? Identificación y evolución en imagenes landsat y radar ERS. *Soc. Geol. Perú* 1, 449–454.

Harpel, C., da Silva, S., and Salas, G. (2011). The 2-ka eruption of Misti volcano, southern Peru -The most recent plinian eruption of Arequipa's iconic volcano. *Geol. Soc. Amer Spec. Pap.* 484, 1–72.

Hasenaka, T., and Carmichael, I. S. (1985). The cinder cones of Michoacán-Guanajuato, central Mexico: Their age, volume and distribution, and magma discharge rate. *J. Volcanol. Geotherm. Res.* 25, 105–124. doi:10.1016/0377-0273(85)90007-1

Huaman-Rodrigo, D., Chorowicz, J., Guillande, R., Antallaca, A., Caceres, R., and Aguilar, A. (1993). "Remote Sensing contribution on seismotectonic hazard in a volcanic active area (Nevado Sabancaya, southern Peru)," in *Int. Symp. Andean geodynamics ISAG*, 373–376.

INGEMMET (2014). GEOCATMIN, Sistema de Información Geológico y Catastral Minero. *Ingemmet, Manual de Uso* 36.

INGEMMET (2021). Evaluación de peligros volcánicos por caída de ceniza en el Distrito de Lluta. Distrito de Lluta, provincia de Caylloma, departamento Arequipa: Lima. *Ingemmet, Inf. Técnico N°* 7205, 40.

James, M. R., Carr, B., D'Arcy, F., Diefenbach, A., Dietterich, H., Fornaciai, A., et al. (2020). Volcanological applications of unoccupied aircraft systems (UAS): Developments, strategies, and future challenges. *Volcanica* 3 (1), 67–114. doi:10.30909/vol.03.01.67114

Japura, S. (2018). *Estudio estratigráfco y sedimentológico del depósito de caída pliniana de la erupción del volcán Huaynaputina del año 1600 d.C. Tesis de Ingeniero Geólogo*. Puno: Universidad Nacional del Altiplano, 192.

Jenks, W. (1948). *Geología de la hoja de Arequipa al 200000*. Boletín: Carta Nacional.

Jenks, W. (1946). Tertiary and Quaternary vulcanism in southern Peru. *Geol. Soc. Am. Bull.* 57, 1209.

Jourdan, F., Renne, P. R., and Reimold, W. U. (2009). An appraisal of the ages of terrestrial impact structures. *Earth Planet. Sci. Lett.* 286, 1–13. doi:10.1016/j.epsl.2009.07.009

Le Bas, M. J., Le Maitre, R. W., Strakeisen, A., and Zanettin, B. (1986). A chemical classification of volcanic rocks based on Total Alkali Silica Diagram. *J. Pet.*. 27, 745–750.

Macdonald, G. A. (1972). *Volcanoes*. Englewood Cliffs, New Jersey, Prentice-Hall. 87.

Mamani, M., Wörner, G., and Semperé, T. (2010). Geochemical variation in igneous rocks of the central andean orocline (13 °S to 18 °S): Tracing crustal thickening and magmas generation through time and space. *Geol. Soc. Amer Bull.* 97, 241–254.

Mariño, J., Thouret, J. C., Cabrera, M., Aguilar, R., Manrique, N., Edwards, B., et al. (2020). *Geología y evaluación de los peligros del complejo volcánico Nevado Coropuna*. Lima: Boletín Geológico, INGEMMET, 145.

Mering, C., Huaman-Rodrigo, D., Chorowicz, J., Deffontaines, B., and Guillande, R. (1996). New data on the geodynamics of southern Peru from computerized analysis of SPOT and SAR ERS-1 images. *Tectonophysics* 259, 153–169. doi:10.1016/0040-1951(96)00034-0

Murcia, H., and Németh, K. (2020). "Effusive monogenetic volcanism." in *Updates in Volcanology - transdisciplinary nature of volcano science*. (London: IntechOpen). doi:10.5772/intechopen.94387

Németh, K., and Kereszturi, G. (2015). Monogenetic volcanism: Personal views and discussion. *Int. J. Earth Sci.* 104, 2131–2146. doi:10.1007/s00531-015-1243-6

Németh, K. (2010). "Monogenetic volcanic fi elds: Origin, sedimentary record, and relationship with polygenetic volcanism," in *What is a volcano?* Editors E. Cañón-Tapia and A. Szakács (Boulder: Geological Society of America Special Paper), 470, 43–66. doi:10.1130/2010.2470(04

Niespolo, E. M., Rutte, D., Deino, A. L., and Renne, P. R. (2017). Intercalibration and age of the Alder Creek sanidine 40Ar/39Ar standard. *Quat. Geochronol.* 39, 205–213. doi:10.1016/j.quageo.2016.09.004

Norabuena, E., Leffier-Griffin, L., Mao, A., Dixon, T., Stein, S., Sacks, S., et al. (1998). Space geodetic observations of nazca-south America convergence across the central Andes. *Science* 279, 358–362. doi:10.1126/science.279.5349.358

Paquereau-Lebti, P., Fornari, M., Roperch, P., Thouret, J.-C., and Macedo, O. (2008). Paleomagnetic, magnetic fabric properties, and $^{40}Ar/^{39}Ar$ dating, of Neogene - Quaternary ignimbrites in the Arequipa area, Southern Peru. Flow directions and implications for the emplacement mechanisms. *Bull. Volc* 70, 977–997.

Paquereau-Lebti, P., Thouret, J.-C., Wörner, G., and Fornari, M. (2006). Neogene and quaternary ignimbrites in the area of Arequipa, southern Peru: Stratigraphical and petrological correlations. *J. Volcanol. Geotherm. Res.* 154, 251–275. doi:10.1016/j.jvolgeores.2006.02.014

Peccerillo, A., and Taylor, S. R. (1976). Geochemistry of Eocene calc-alkaline volcanic rocks from the Kastamonu area, northern Turkey. Contrib. *Mineral. Pet.* 58, 63–81.

Planagumà-Guàrdia, L., Martí-Molist, J., and Vila-Subirós, J. (2022). Conservation of the geological heritage of volcanic fields: La Garrotxa volcanic zone natural park, Spain. *Geoheritage* 14, 39. doi:10.1007/s12371-022-00677-w

Prival, J. M., Thouret, J-C., Japura, S., Gurioli, L., Bonadonna, C., Mariño, J., et al. (2020). New insights into eruption source parameters of the 1600 CE Huaynaputina Plinian eruption, Peru. *Bull. Volcanol.* 82, 7. doi:10.1007/s00445-019-1340-7

Ramos, V. (2010). The tectonic regime along the Andes: Present-day and mesozoic regimes. *Geol. J.* 45 (1), 2–25. doi:10.1002/gj.1193

Renne, P. R., Balco, G., Ludwig, K. R., Mundil, R., and Min, K. (2011). "Response to the comment by W.H. Schwarz et al. on," in *Joint determination of 40K decay constants and 40Ar */40K for the Fish Canyon sanidine standard, and improved accuracy for 40Ar/39Ar geochronology*. Editors, 75, 5097–5100.*Geochimica Cosmochimica Acta*17

Rivera, L. (2021). "Mapeo Tridimensional del volcán Nicholson, Perú, mediante la inversión del vector magnético esparcido en coordenadas esféricas," in *Report (unpubl.), IGCP-692 project: Geoheritage for geohazard resilience*, 93.

Rivera, M., Thouret, J.-C., Mariño, J., Berolatti, R., and Fuentes, J. (2010). Characteristics and management of the 2006–2008 volcanic crisis at the Ubinas volcano (Peru). *J. Volcanol. Geotherm. Res.* 198 (1-2), 19–34. doi:10.1016/j.jvolgeores.2010.07.020

Rivera, M., Thouret, J.-C., Samaniego, P., and Le Pennec, J. L. (2014). The 2006–2009 activity of the Ubinas volcano (Peru): Petrology of the 2006 eruptive products and insights into Genesis of andesite magmas, magma recharge and plumbing system. *J. Volcanol. Geotherm. Res.* 270, 122–141. doi:10.1016/j.jvolgeores.2013.11.010

Rivera, M., Vílchez, M., and Vela, J. (2018). *Peligros por huaicos en la ciudad de Arequipa. En: Taller Internacional Fortalecimiento de capacidades para mitigar los impactos de huaicos en Perú, Lima y Arequipa, Perú, 15-19 octubre 2018: Libro de Resúmenes*. Arequipa: INGEMMET, 45–49.

Rodríguez Rey, A., Calleja, L., Suárez del Río, L., Ruiz de Argandoña, V., Díez Sarriá, I., and Sánchez Delgado, N. (2004). Procedimiento estereológico para la cuantificación del tamaño de grano de rocas en 2-D: Aplicación a la interpretación petrofísica de la velocidad de corte de granitos con útiles diamantados. *Trab. Geol.* 24, 147–152.

Samaniego, P., Rivera, M., Mariño, J., Guillou, H., Liorzou, C., Zerathe, S., et al. (2016). The eruptive chronology of the Ampato-Sabancaya volcanic complex (southern Peru). *J. Volcanol. Geotherm. Res.* 323, 110–128. doi:10.1016/j.jvolgeores.2016.04.038

Sempere, T., and Jacay, J. (2006). *Estructura tectónica del Sur del Perú (Antearco, arco y Altiplano suroccidental)*. Lima: XIII Congreso Peruano de Geología, Extended Abstracts, 324–327.

Sempere, T., Noury, M., Garcia, F., and Bernet, M. (2014). "Elementos para una actualización de la estratigrafía del Grupo Moquegua, sur del Perú," in *XVII congreso peruano de Geología, Lima, extended abstracts, digital file "Sempere* (Lima: T", Soc Geol Perú).

Siebe, C., Schaaf, P., Carlotto, V., and Gomez, J. C. (2006). Radiocarbon ages and composition of holocene-late Pleistocene monogenetic kimsachata and oroscocha volcanoes in cusco, Peru. *Cities Volcanoes* 4, 23–27.

Stern, C. R. (2004). Active andean volcanism: Its geologic and tectonic setting. *Rev. Geol. Chile* 31 (2), 161–206. doi:10.4067/s0716-02082004000200001

Sun, S., and McDonough, W. F. (1989). Chemical and isotopic systematics of oceanic basalts: Implications for mantle composition and processes. *Geol. Soc. Amer Spec. Pap.* 42, 313–345. doi:10.1144/gsl.sp.1989.042.01.19

Thorpe, R. S., Francis, P. W., Hammil, M., and Baker, M. B. (1982). in *The Andes*. Editor R. S. Thorpe (New York: Andesites), 187–205.

Thouret, J.-C., Finizola, A., Fornari, M., Legeley-Padovani, A., Suni, J., and Frechen, M. (2001). Geology of el Misti volcano near the city of Arequipa, Peru. *Geol. Soc. Am. Bull.* 113 (12), 1593–1610. doi:10.1130/0016-7606(2001)113<1593:goemvn>2.0.co;2

Thouret, J.-C., Jicha, B., Paquette, J.-L., and Cubukcu, E. (2016). A 25 Myr chronostratigraphy of ignimbrites in South Peru. Implications for the volcanic history of the Central Andes. *J. Geol. Soc. Lond.* 173, 734–756. doi:10.1144/jgs2015-162

Torres, I., Németh, Ká., Ureta, G., and Aguilera, F. (2020). Characterization, origin, and evolution of one of the most eroded mafic monogenetic fields within the central Andes: The case of El País lava flow field, northern Chile. *J. S. Am. Earth Sci.* 105, 102942. doi:10.1016/j.jsames.2020.102942

Valentine, G. A., and Gregg, T. K. P. (2008). Continental basaltic volcanoes - processes and problems. *J. Volcanol. Geotherm. Res.* 177, 857–873. doi:10.1016/j.jvolgeores.2008.01.050

van Wyk de Vries, B., and Merle, O. (1998). Extension induced by volcanic loading in regional strike-slip zones. *Geol.* 26, 983–986. doi:10.1130/0091-7613(1998)026<0983:eibvli>2.3.co;2

Vargas, L. (1970). Geología del Cuadrángulo de Arequipa. *Boletín del Servicio de Geología y Minería* 24, 64.

Global Volcanism Program (2013). in *Cerro Nicholson (354008) in volcanoes of the World*. Editor E. Venzke (Smithsonian Institution). Downloaded https://volcano.si.edu/volcano.cfm?vn=354008 (Accepted Jun 30, 2022).

Vereb, V., van Wyk de Vries, B., Guilbaud, M-N., and Karátson, D. (2020). The urban geoheritage of clermont-ferrand: From inventory to management. *Quaest. Geogr.* 39 (3), 5–31. doi:10.2478/quageo-2020-0020

Vicente, J.-C., Sequeiros, F., Valdivia, M., and Zavala, J. (1982). El sobre-escurrimiento de Cincha-lluta: Elemento del accidente mayor andino al NW de Arequipa. *Bol. Soc. Geol. Perú* 61, 67–99.

Williams, H., and McBirney, A. R. (1979). *Volcanology*. San Francisco: Freeman, 397.

Wilson, J. J. (1963). Cretaceous stratigraphy of the central Andes of Peru. *Am. Assoc. Petrol. Geol. Bull.* 47, 1–34.

Wilson, M. (1986). *Igneous petrogenesis*. London: Unwyn Hyman, 456.

Wood, C. A. (1979). "Monogenetic volcanoes in terrestrial planets," in Proceedings of the 10 th Lunar and Planetary Science Conference.

Wörner, G., Mamani, M., and Blum-Oeste, M. (2018). Magmatism in the central Andes. *Elem. (Que).* 14, 237–244. doi:10.2138/gselements.14.4.237